Advances in Nano Research, *Vol. 11, No. 4 (2021) 361-380*
https://doi.org/10.12989/anr.2021.11.4.361

Free vibration analysis of FG porous joined truncated conical-cylindrical shell reinforced by graphene platelets

Faraz Kiarasi[1a], Masoud Babaei[1b], Somayeh Mollaei[2], Mokhtar Mohammadi[3] and Kamran Asemi[*4]

[1]*Department of Mechanical Engineering, University of Eyvanekey, Eyvanekey, Semnan, Iran*
[2]*Department of Civil Engineering, University of Bonab, Bonab, East Azerbaijan, Iran*
[3]*Department of Information Technology, College of Engineering and Computer Science, Lebanese French University, Kurdistan Region, Iraq*
[4]*Department of Mechanical Engineering, Islamic Azad University, North Tehran Branch, Tehran, Iran*

(*Received January 9, 2021, Revised June 12, 2021, Accepted August 9, 2021*)

Abstract. Natural frequency analysis of functionally graded porous joined truncated conical–cylindrical shell reinforced by graphene platelet is investigated in this paper. The structure is consisting of a layered model with five kinds of distribution of graphene platelets in a metallic matrix containing open-cell interior pores. To calculate the effective properties of the porous nanocomposite joined shell, the generalized rule of mixture and the modified Halpin-Tsai equations are employed. Four different porosity distributions are assumed along the shell thickness: two kinds of symmetric functionally graded distributions, non-symmetric functionally graded distributions and uniform distribution of porosity. Graded finite element method (GFEM) based on Rayleigh-Ritz energy formulation has been used to solve 2D- axisymmetric elasticity equations. A parametric study is also conducted to show the effects of different geometric parameters, boundary conditions, weight fraction of graphene platelets, porosity coefficient, distribution of porosity and dispersion pattern of graphene platelets on the natural frequencies and mode shapes of the structure.

Keywords: FG porous; graded finite element method; graphene platelets; joined truncated conical–cylindrical shell; natural frequency analysis

1. Introduction

Cylindrical and conical shell structures are utilizing in various industries and engineering applicants. However, joined shells comprising different cylindrical, conical and spherical shell sections are employed, especially in submarine structures and aerospace engineering. This kind of structure is mostly under aerodynamic forces. Therefore, it is of significance and value to prevent the resonance phenomenon in these structures with sensitive applications in engineering. The revolution of natural frequency behavior of structures with different geometries, including conical, cylindrical, and spherical shells, has been the title of several works for a long time. Therefore, the subject is investigated in numerous textbooks, for instance Leissa (1993), Qatu (2004) and Soedel (2004). However, the natural frequencies characteristics of joined shells are less considered in the open scientific literature because of the number of equations and difficulties that may appear while using the boundary and continuity conditions. Vibrations of joined shells compared to the free vibrations of a single shell are less reported. Thus, a brief overview of the papers dealing with such titles is presented here. Kang (2012) investigated the natural frequency of a joined cylindrical–conical shell according to framework of 3-D elasticity theory. The multi-term Ritz method is employed to solve the governing equations. Qu *et al*. (2013) studied the natural frequency of a joined cylindrical–conical shell system by using Reissner–Naghdi theory as the basic theoretical supposition and considering classical or non-classical boundary conditions. The interface continuity and geometric boundary conditions were almost performed by using a generalized variational principle and least-squares weighted residual procedure. Shakouri and Kouchakzadeh (2014) analyzed the vibration behavior of a thin conical–conical shell system utilizing the power series solution system. This paper also includes an experimental study for the case of a joined conical-conical shell system with both ends free condition. Free and forced vibration of a ring-stiffened joined conical-cylindrical shell was presented by Chen *et al*. (2015). They also used power series, wave functions and Bessel functions to indicate the displacement functions of each part. Natural frequency analysis of a joined shell system consisted of two conical shells was done by Bagheri *et al*. (2017). This work assumed that the joined shell is made from a linearly elastic isotropic homogeneous material. They used first-order theory of shells to capture the shear deformations through the thickness and rotary inertias. Also, the Donnell type of kinematic assumption was considered to establish the general motion equations. The resulted equations were discretized by applying the semi-analytical generalized differential quadrature (GDQ) method. Lee (2018) developed a free vibration analysis of

*Corresponding author, Assistant Professor,
E-mail: K.asemi@iau-tnb.ac.ir
[a] Lecturer, E-mail: f.kiarasi@eyc.ac.ir
[b] Lecturer, E-mail: masoudbabaei@eyc.ac.ir.

ISSN: 2287-237X (Print), 2287-2388 (Online)

joined conical-cylindrical shells. They used the first-order shell deformation theory, also depicted the deflections and rotations by the expansions of Chebyshev polynomials and Fourier series. The free vibration features of a joined shell system comprised of three segments, two conical shells at the ends and a cylindrical shell at the middle, were presented by Bagheri *et al.* (2018). The whole model was made from an isotropic homogeneous material. In this work, by using first-order shell deformation theory and the Donnell type of kinematic relation, the governing equations of motion were derived. They also considered the intersection continuity conditions for rotations, forces, displacements and moments among two adjacent shells as well as boundary conditions at the ends of the system. Free vibration response of a joined shell system, including cylindrical and spherical shells made of a functionally graded material (FGM), was analyzed by Bagheri *et al.* (2020). The shell was assumed to be graded through the thickness. Moreover, some parametric studies were conducted for the combined moderately thick cylindrical–spherical shell system to explore the influence of power-law index and geometric properties. Irie *et al.* (1984) presented an analysis for the free vibration of joined conical-cylindrical shells. The governing equations of vibration of a conical and a cylindrical shell were derived as a coupled set of first-order differential equations by utilizing the transfer matrix of the shell. Gia Ninh *et al.* (2020) employed a novel numerical approach to investigate natural frequency of functionally graded joined conical–cylindrical–conical shells reinforced by carbon nanotubes based on Donnell type theory. They compared the results with experimental and finite element analysis. Wu *et al.* (2012) utilized a domain decomposition method to investigate the vibrational behavior of the combined cylindrical-spherical shell with considering various boundary conditions. The boundary equations were placed into the energy functional of the combined shell, and the constraint equations were obtained from interface continuity conditions among two adjacent shell subdomains. Fourier series and Chebyshev orthogonal polynomials were employed as the admissible displacement functions for each part in the circumferential direction and axial direction to gain the discretization equations of motion of the system. An investigation of the free vibrational behavior of joined composite sandwich conical-conical shells under external lateral pressure was presented by Soureshjani *et al.* (2020a). In this research, the corresponding equations were derived by employing the first-order shear deformation theory (FSDT), and by applying Hamilton's principle, free vibration equations were extracted. For each segment, GDQ method was adopted to discretize the governing equations, accompanied by the related boundary and continuity conditions in a meridian direction. Soureshjani *et al.* (2020b) investigated the temperature influences on the natural frequency of carbon nanotube-reinforced composite (CNTRC) joined conical-conical shells. These nanotubes were embedded through the thickness uniformly or functionally. They used FSDT and von Karman types of geometrical nonlinearity applied in Hamilton's principle to derive the governing equations of motion. They also used the GDQ procedure to discretize the governing equations.

In terms of material, nowadays, there is a high demand for high structural implementation and multi-functionality with great mechanical properties. The cellular structures made of porous materials having valuable properties, e.g. lightweight, heat resistance, and excellent energy absorption, have been considerably used in various engineering implementations (Smith *et al.* 2012 and Lefebvre *et al.* 2008). Many investigations have been conducted in this field; among them for instance, Akbas (2018b) employed the finite element approach to investigate the forced vibration analysis of functionally graded porous deep beams based on plane solid continua model. Babaei *et al.* (2019) studied the free and forced vibration of saturated FG porous beam based on third-order shear deformation theory by employing finite element method. Akbas (2017d) presented an analytical solution for vibration and static analysis of functionally graded porous plates based on FSDT. Akbas (2017c) applied the finite element model to investigate the thermal influence on vibration of functionally graded deep beams with porosity based on FSDT. Post-buckling behavior of functionally graded porous beams was presented by Akbas (2017b). Akbas (2018a) investigated geometrically nonlinear analysis of functionally graded porous beams based on Timoshenko beam theory and by employing finite element and Newton Raphson methods. Babaei *et al.* (2021) investigated the dynamic analysis of saturated FG porous truncated cone based on elasticity theory and by employing finite element method. Babaei *et al.* (2020) studied the free vibration and static responses of saturated FG porous elliptical plate based on 3D elasticity theory and by applying finite element method. Akbas (2017a) investigated the stability of porous plate based on classical plate theory and by employing GDQM.

However, the presence of internal pores and holes in the metal matrix induces a remarkable reduction of the stiffness of structures (Xia *et al.* 2013 and Wang *et al.* 2017). Compensating this limitation, reinforcement with CNTs (Iijima 1991, Liew *et al.* 2015 and Nguyen *et al.* 2019) or graphene nano-platelets (GPLs) (Mittal *et al.* 2015) into lightweight materials is taken into account as an excellent and useful approach to strengthen their mechanical features. In addition, this reinforcement also causes them to keep their potential for lightweight structures (Duarte *et al.* 2015). In comparison to CNTs, GPLs have revealed substantial abilities to choose a proper reinforcement candidate (Rafiee *et al.* 2009) due to they have excellent mechanical properties with lower fabricating cost, larger specific surface area and 2-D geometry. To boost the efficiency of structures, FG porous structures reinforced by GPLs have been suggested in the literature to determine the favorable mechanical properties by controlling the size and density of porosities as well as patterns of internal pores and GPLs (Hassani *et al.* 2012). In this sense, Bahaadini *et al.* (2019) investigated the vibration of FG porous truncated conical shell reinforced by GPLs. They found that the natural frequencies of nanocomposite conical shell can be reduced by raising the porosity coefficient. Furthermore, the geometry, size and weight fraction of GPLs have substantial

effects on the natural frequencies. Yan *et al*. (2020) presented the natural frequency of conical shell structures reinforced by GPLs. The elastic properties of the nanocomposite were obtained by utilizing the Halpin-Tsai micromechanics model. Galerkin method was employed in addition to beam mode shapes as weighting functions. It was shown that Donnell's shell theory is efficient, robust and accurate in terms of nanocomposite problems. Asemi *et al*. (2020) comprehensively investigated the static, free and forced vibration of FG porous annular sector plate reinforced by GPLs based on the FSDT. Rayleigh-Ritz energy formulation was applied to achieve the governing equations of motion, and FEM was employed to solve the governing equations. Based on FSDT and Halpin Tsai model, wave propagation of FG porous shell reinforced by GPLs is studied by Ebrahimi *et al*. (2019). According to Euler-Bernoulli's theory and by applying the Galerkin method, dynamic analysis of FG porous arches reinforced by GPLs was investigated by Zhao *et al*. (2020). Gao *et al*. (2018) investigated nonlinear free vibration of FG porous plates reinforced by GPLs based on classical plate theory and employing Halpin-Tsai relations and Von Kármán strain-displacement assumption. Based on FSDT and generalized Halpin- Tsai model, vibration analysis of FG porous cylindrical shells by considering spinning motion reinforced by GPLs were presented by Dong *et al*. (2018). Nematollahi *et al*. (2020) studied nonlinear vibration of FG composite sandwich beams reinforced by GPLs based on higher order beam theory and employing Von Kármán strain-displacement assumption. Besseghier *et al*. (2015) studied nonlinear vibration of a zigzag single-walled carbon nanotube (SWCNTs) embedded in a polymer matrix based on the Winkler model. The vibration of nanoparticles that usually employs in the reinforced structure is investigated separately. For instance: Khadimallah *et al*. (2020) studied vibration of SWCNTs according to Hamilton's variational principle and using Galerkin's method. Hussain *et al*. (2020a) presented a novel approach based on Sander's theory to investigate SWCNTs' vibration under various boundary conditions. In another study, Hussain *et al*. (2020b) investigated the vibration analysis of SWCNTs based on generalized Kelvin's model. Based on higher order theories, free and forced vibration of SWCNTs according to various rod models was presented by Khosravi *et al*. (2020).

The above literature shows that most of the studies are focused on the behavior of porous structures or structures reinforced by GPLs. However, the effect of reinforcing a porous material by GPLs is less investigated. Also, most of researches deal with simple shape structures such as beams, plates and cylindrical or conical shells, and the behavior of complicated shapes such as FG-GPL porous joined shells is not investigated so far. Furthermore, in the most of previous studies, simple shell and plate theories rather than elasticity theory are used to model the problem. Application of 2D axisymmetric elasticity theory allows thickness stretching unlike simple shell theories, and this gives more accurate results, especially for thick shells.

The application of joined shells is in many industries such as aerospace and lightweight structures motivated the authors to study the free vibration behavior joined shell made of FG porous materials reinforced by GPLs. Therefore, in the present research, an efficient numerical model is conducted to study free vibration of joined truncated conical–cylindrical shell reinforced by GPLs. The structure is considered of a multilayer model with uniform and non-uniform dispersion of GPLs in a metallic matrix comprising open-cell interior pores. Four patterns of porosity distributions, that are uniform and two kinds of symmetric and non-symmetric distributions, are assumed along the thickness of the shell. In addition, five different patterns of GPL dispersion patterns are considered through the shell thickness. Two-dimensional axisymmetric elasticity theory and FEM based on Rayleigh–Ritz energy formulation are employed to solve the equations. A parametric study is also conducted to show the effect of various length ratios, different porosity distribution, various semi-vertex angle of the cone, porosity coefficient, GPL dispersion patterns and weight fraction of GPL Nano-fillers and different boundary conditions on the free vibration of the structure.

2. Governing equations:

2.1. Definition of geometry

Considering an FG-GPL porous joined truncated conical-cylindrical shell with total length L = L1 + L2 (L1 and L2 are the length of conical and cylindrical shell, respectively), thickness h, inner radius of small base of cone a, outer radius of the small base of cone b and semi-vertex angle φ as depicted in Fig 1. Axisymmetric cylindrical coordinates (r, z) are assumed through the radial and axial directions, respectively. Also, various porosity distribution and GPLs dispersion patterns are shown in Fig 1.

2.2 Material properties of FG porous joined truncated conical-cylindrical shell reinforced by graphene platelet

Four different porosity distributions are assumed through the shell thickness (Fig. 1). Two types of non-uniform symmetric porosity distribution, non-uniform nonsymmetric distribution and a uniform porosity distribution are considered. In distribution 1, the porosity is symmetric nonlinear, and porosity around the mid-plane is higher rather than the inner and outer surfaces of the shell. In distribution 2, non-uniform symmetric porosity is assumed, and porosity near the inner and outer surfaces is higher rather than the mid-plane. In distribution 3, non-uniform non-symmetric porosity is assumed, and porosity near the outer surface is lower than inner surfaces and the mid-plane. The distribution of material properties considering the effect of porosity for distributions 1, 2 and 3 are given in Eqs. (1)-(3), respectively. The mathematical representation of mechanical properties for the uniform distribution of porosity is indicated in Eq. (4). Besides, five GPL distribution patterns along the shell thickness are indicated in Fig. 1 and given in Eq. (17) (Babaei and Asemi 2020).

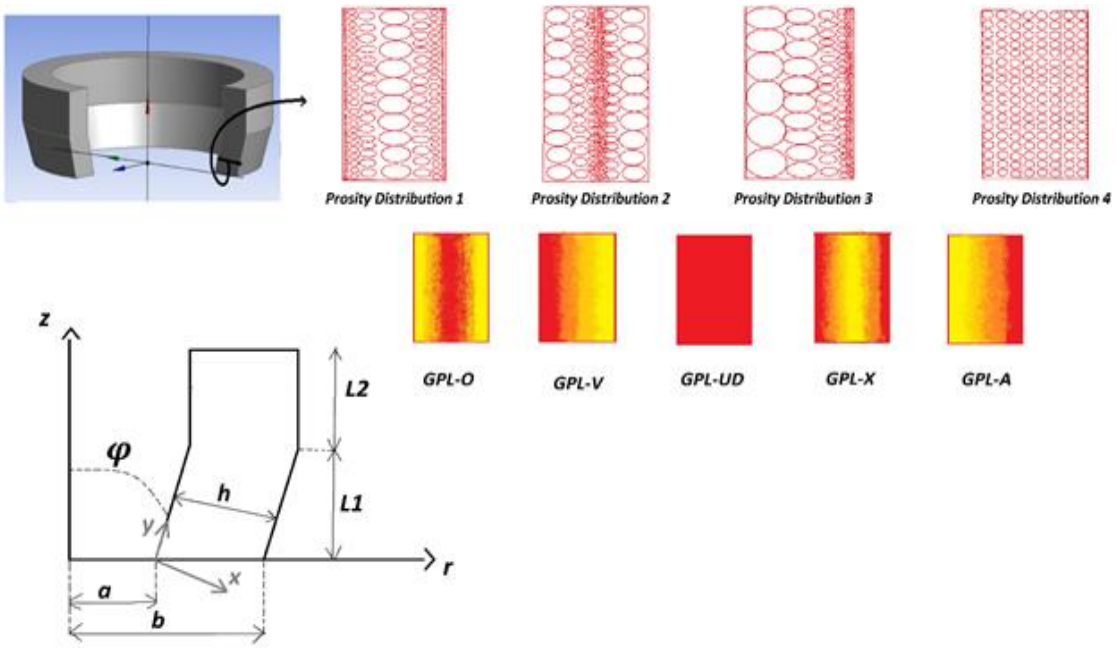

Fig. 1 Geometry of joined truncated conical-cylindrical shell for various porosity distribution and different GPL dispersion patterns through the thickness direction

Porosity distribution 1 (Non-uniform symmetric I):

$$\begin{aligned} E(x) &= E^*[1 - e_0 cos(\pi/2 - \pi x/h)] \\ G(x) &= G^*[1 - e_0 cos(\pi/2 - \pi x/h)] \\ \rho(x) &= \rho^*[1 - e_m cos(\pi/2 - \pi x/h)] \end{aligned} \quad (1)$$

Porosity distribution 2 (Non-uniform symmetric II):

$$\begin{aligned} E(x) &= E^*\left[1 - e_0^*\left(1 - \cos(\pi/2 - \pi x/h)\right)\right] \\ G(x) &= G^*\left[1 - e_0^*\left(1 - \cos(\pi/2 - \pi x/h)\right)\right] \\ \rho(x) &= \rho^*\left[1 - e_m^*\left(1 - \cos(\pi/2 - \pi x/h)\right)\right] \end{aligned} \quad (2)$$

Porosity distribution 3 (Non-uniform non-symmetric):

$$\begin{aligned} E(x) &= E^*[1 - e_0 \cos(\pi x/2 * h)] \\ G(x) &= G^*[1 - e_0 \cos(\pi x/2 * h)] \\ \rho(x) &= \rho^*[1 - e_m \cos(\pi x/2 * h)] \end{aligned} \quad (3)$$

Uniform porosity distribution (Porosity distribution 4):

$$\begin{aligned} E &= E^*\Theta \\ G &= G^*\Theta \\ \rho &= \rho^*\Theta' \end{aligned} \quad (4)$$

The following equations are applied for evaluating x $(0 \le x \le h)$: (Babaei and Asemi 2020).

$$\begin{aligned} x &= \sqrt{(r_n - r_{in})^2 + (z_n - z_{in})^2} \\ r_{in} &= \frac{\left(tan(\pi - \varphi) r_n - z_n - a\, tan\left(\frac{\pi}{2} - \varphi\right)\right)}{tan(\pi - \varphi) - tan\left(\frac{\pi}{2} - \varphi\right)} \\ z_{in} &= tan\left(\frac{\pi}{2} - \varphi\right)(r_{in} - a) \end{aligned} \quad (5)$$

when $\varphi = 0$ (cylinder) x = r_n-a, h = b-a.

In which x indicates the normal distance of points along the thickness direction of the conical segment from the inner surface, r_n and z_n are the radius and height of each point in the domain, r_{in} and z_{in} are the radius and height of points at the inner surface. Moreover, $E(x)$, $G(x)$, $\rho(x)$ $E*$, $G*$ and $\rho*$ being the elasticity modulus, rigidity modulus and mass density of porous nanocomposite shell, the elasticity modulus, rigidity modulus and mass density of GPL shell without interior cavities, respectively. Also, e_0 and e_0^* ($0 \le e_0(e_0^*) < 1$) introduce the coefficients of porosity for distribution 1, 3 and 2, respectively. e_m and e_m^* indicate the same coefficients of mass density for the mentioned distributions. Θ and Θ' stand for the variables of uniform porosity distribution. As the size and density of interior cavities increases, the porosity increases, and consequently, causes a reduction in the material properties.

The influence of material properties dedicated to open-cell metal foams (Gibson and Ashby 1982, Ashby et al. 2000 and Choi and Lakes 1995) are presented in Eq. (6). Thus, Eq. (6) is utilized to derive the relation between the porosity coefficients and mass density coefficients for porosity patterns in Eq. (7)

$$\frac{E(x)}{E^*} = \left(\frac{\rho(x)}{\rho^*}\right)^2 \quad (6)$$

$$\begin{cases} 1 - e_m \cos\left(\frac{\pi}{2} - \frac{\pi x}{h}\right) = \sqrt{1 - e_0\left(\frac{\pi}{2} - \frac{\pi x}{h}\right)} \\ 1 - e_m^*(1 - \cos\left(\frac{\pi}{2} - \frac{\pi x}{h}\right)) = \sqrt{1 - e_0^*(1 - \cos\left(\frac{\pi}{2} - \frac{\pi x}{h}\right)} \\ \Theta' = \sqrt{\Theta} \end{cases} \quad (7)$$

We assume that the mass of shell with different porosities and GPL dispersions are identical, consequently:

$$\begin{cases} 1-e_m\cos\left(\frac{\pi}{2}-\frac{\pi x}{h}\right)=\sqrt{1-e_0\left(\frac{\pi}{2}-\frac{\pi x}{h}\right)} \\ 1-e_m^*(1-\cos\left(\frac{\pi}{2}-\frac{\pi x}{h}\right))=\sqrt{1-e_0^*(1-\cos\left(\frac{\pi}{2}-\frac{\pi x}{h}\right)} \\ \Theta'=\sqrt{\Theta} \end{cases} \quad (8)$$

which are employed to calculated e_0^* and Θ with a known value of e_0. It can be observed that e_0^* rises by enhancing e_0. Also, when e_0 reaches 0.6,e_0^* (= 0.9612) is near to the upper bound. Therefore, $e_0 \in [0,0.6]$ is employed in the present research.

According to Halpin-Tsai micromechanics model (Tjong 2013), elastic modulus of the nanocomposite $E*$ without interior cavities is expressed as:

$$E^* = \frac{3}{8}\left(\frac{1+\varepsilon_L^{GPL}\eta_L^{GPL}V_{GPL}}{1-\eta_L^{GPL}V_{GPL}}\right)E_m + \frac{5}{8}\left(\frac{1+\varepsilon_W^{GPL}\eta_W^{GPL}V_{GPL}}{1-\eta_W^{GPL}V_{GPL}}\right) \quad (9)$$

$$\varepsilon_L^{GPL}=\frac{2l_{GPL}}{t_{GPL}} \quad (10)$$

$$\varepsilon_W^{GPL}=\frac{2w_{GPL}}{t_{GPL}} \quad (11)$$

$$\eta_L^{GPL}=\frac{E_{GPL}-E_m}{E_{GPL}+\varepsilon_L^{GPL}E_m} \quad (12)$$

$$\eta_L^{GPL}=\frac{E_{GPL}-E_m}{E_{GPL}+\varepsilon_W^{GPL}E_m} \quad (13)$$

where E_{GPL} , E_m , l_{GPL}, W_{GPL} , t_{GPL} and V_{GPL} being the elasticity modulus of GPLs, the elasticity modulus of metallic matrix, length, width and thickness of nano-filler platelets, and the volume content of GPLs, respectively. The rule of mixture (Shen et al. 2017) is used to calculate the Poisson's ratio and mass density of the nanocomposite:

$$\rho^* = \rho_{GPL}V_{GPL}+\rho_m(1-V_{GPL}) \quad (14)$$

$$v^* = v_{GPL}V_{GPL}+v_m(1-V_{GPL}) \quad (15)$$

where ρ_{GPL}, ρ_m, ν_{GPL} and υ_m are the mass density of GPL, mass density of metal matrix, Poisson's ratio of GPL and Poisson's ratio of metal matrix, respectively. Also, it is assumed that Poisson's ratio is constant for open-cell metal foams (Wicklein and Thoma 2005). The $G*$ rigidity modulus of the nanocomposite expresses as bellow:

$$G^*=\frac{E^*}{2(1+v^*)} \quad (16)$$

V_{GPL} changes across the shell thickness introduced in the Eq. (17) for various dispersion patterns.

$$V_{GPL}(x)=\begin{Bmatrix} t_{i1}[1-cos(\frac{\pi}{2}-\frac{\pi x}{h})]GPLX \\ t_{i2}[1-cos(\frac{\pi x}{2h})]GPLA \\ t_{i3}GPLUD \\ t_{i4}[cos(\frac{\pi x}{2h})]GPLV \\ t_{i5}[sin(\frac{\pi x}{h})]GPLO \end{Bmatrix} \quad (17)$$

where t_{i1}, t_{i2}, t_{i3}, t_{i4} and t_{i5} denote the upper limit of the V_{GPL}, and i =1, 2, 3,4 corresponding various porosity distributions 1, 2,3 and uniform distribution. V_{GPL}^T is estimated by applying the nano-filler weight fraction Δ_{GPL}into Eq. (18), then it is used to derive t_{i1}, t_{i2}, t_{i3}, t_{i4} and t_{i5} by Eq. (19).

$$V_{GPL}^T=\frac{\Delta_{GPL}\rho_m}{\Delta_{GPL}\rho_m+\rho_{GPL}-\Delta_{GPL}\rho_{GPL}} \quad (18)$$

$$V_{GPL}^T\int_{-h/2}^{h/2}\frac{\rho(x)}{\rho^*}dx = \begin{cases} t_{i1}\int_{-h/2}^{h/2}[1-cos(\pi/2-\pi x/h)]\frac{\rho(x)}{\rho^*}dx \\ t_{i2}\int_{-h/2}^{h/2}[1-cos(\pi x/2h)]\frac{\rho(x)}{\rho^*}dx \\ t_{i3}\int_{-h/2}^{h/2}\frac{\rho(x)}{\rho^*}dx \\ t_{i4}\int_{-h/2}^{h/2}[cos(\pi x/2h)]\frac{\rho(x)}{\rho^*}dx \\ t_{i5}\int_{-h/2}^{h/2}[sin(\pi x/h)]\frac{\rho(x)}{\rho^*}dx \end{cases} \quad (19)$$

3. Deriving governing equations of motion

Consider a joined truncated conical-cylindrical shell as depicted in Fig. 1. As obvious, the shell is 3-D while the geometry of the cone is not a function of the circumferential direction. Therefore, the cone can be reduced to 2D-axisymmetric elasticity equations. Consequently, the circumferential displacement, shear stresses and strains in r-θ and θ-z planes become zero. Thus, by omitting the body forces, the equations of motion in term of stresses $\sigma_{ij}\ (i.j)=r.\theta.z$ in axisymmetric cylindrical coordinates are expressed as following:

$$\sigma_{rr,r}+\frac{1}{r}(\sigma_{rr}-\sigma_{\theta\theta})+\tau_{rz,z}=\rho(x)u_{,tt} \quad (20)$$

$$\tau_{rz,r}+\sigma_{zz,z}+\frac{1}{r}\tau_{rz}=\rho(x)v_{,tt} \quad (21)$$

The strain-displacement relations are as:

$$[\varepsilon]=\begin{bmatrix}\varepsilon_{rr}\\ \varepsilon_{\theta\theta}\\ \varepsilon_{zz}\\ \varepsilon_{rz}\end{bmatrix}=\begin{bmatrix}u_{,r}\\ \frac{1}{r}u\\ v_{,z}\\ \frac{1}{r}(u_{,z}+v_{,r})\end{bmatrix} \tag{22}$$

In which u and v being the displacement components through the radial and axial directions. Eq. (22) can be introduced as:

$$[\varepsilon]=[d]\{f\},\ \{f\}=\begin{Bmatrix}u\\ v\end{Bmatrix},\ [d]=\begin{bmatrix}\frac{\partial}{\partial r} & 0\\ \frac{1}{r} & 0\\ 0 & \frac{\partial}{\partial z}\\ \frac{1}{2}\frac{\partial}{\partial z} & \frac{1}{2}\frac{\partial}{\partial r}\end{bmatrix} \tag{23}$$

Matrix form of the stress-strain relation resulted from the Hook's law for a linearly elastic material is

$$[\sigma]=\begin{bmatrix}\sigma_{rr}\\ \sigma_{\theta\theta}\\ \sigma_{zz}\\ \tau_{rz}\end{bmatrix}=[D][\varepsilon] \tag{24}$$

where the coefficients of elasticity are as (Asemi et al 2014):

$$[D]=\frac{E(x)}{(1+\upsilon)(1-2\upsilon)}\begin{bmatrix}1-\upsilon & \upsilon & \upsilon & 0\\ \upsilon & 1-\upsilon & \upsilon & 0\\ \upsilon & \upsilon & 1-\upsilon & 0\\ 0 & 0 & 0 & \frac{1-2\upsilon}{2}\end{bmatrix}= \tag{25}$$
$$E(x)\Lambda$$

In Eq. (25), E and υ denote the Young's modulus and Poisson's ratio which are function of x coordinates. The constant part of matrix D is defined as $\boldsymbol{\Lambda}$.

For a shell that is clamped on its two end edges, the displacement boundary conditions are considered as:

B.C 1:

$$u, v(\mathrm{r},0)= u, v(\mathrm{r},\mathrm{L})= 0 \tag{26}$$

and for a shell which is clamped at its outer surface, one may write

B.C 2:

$$\mathrm{u}, \mathrm{v}(r_{out},\mathrm{z})= 0 \tag{27}$$

A combination of Eq. (26) and (27) is related to a shell which is clamed at its two end edges and outer surface (B.C 3).

4. Finite element modeling

In this section, for solving the governing equations, the graded finite element method is applied. In conventional FEM, material property is constant through the element. In GFEM, to treat the material heterogeneity, in addition to displacement field, the material properties of the FG porous of joined truncated conical–cylindrical shell reinforced by GPLs could also be determined from their nodal values. This approach leads to a continuous variation of the material properties through the structure and also obtains more accurate results than dividing the solution domain into homogenous elements. By using the shape functions of quadratic six nodded triangular element in the axisymmetric cylindrical coordinates, the displacement field and material properties for each element (e) in terms of the nodal displacement vector $\{\delta\}$, nodal elasticity modulus E_i and mass density ρ_i and shape function matrix N are as:

$$\begin{aligned}\{q\}^{(e)}=N^e\{\delta\}^e,\quad E&=\sum_{i=1}^{6}E_iN_i=\widehat{\boldsymbol{N}}\boldsymbol{\Xi},\rho\\ &=\sum_{i=1}^{6}\rho_iN_i=\widehat{\boldsymbol{N}}\Re(28)\end{aligned} \tag{28}$$

where $\boldsymbol{\Xi}$ and $\Re$ are respectively vectors of the nodal elasticity moduli and mass densities, and are as:

$$\begin{aligned}\widehat{\boldsymbol{N}}&=[N_1\quad N_2\quad N_3\ N_4\quad N_5\quad N_6],\quad \boldsymbol{\Xi}\\ &=[E_1\quad E_2\quad E_3\quad E_4\quad E_5\quad E_6]^T\\ \Re&=[\rho_1\quad \rho_2\quad \rho_3\ \rho_4\quad \rho_5\quad \rho_6]^T\end{aligned} \tag{29}$$

Substituting Eq. (28) into Eq. (23) results in the strain matrix of element (e) as follows:

$$\{\varepsilon\}^{(e)}=B^{(e)}\{\delta\}^{(e)},\ \{\delta\}^{(e)}=\begin{bmatrix}U_1\\ V_1\\ .\\ .\\ .\\ U_6\\ V_6\end{bmatrix} \tag{30}$$

where $\boldsymbol{B}^{(e)}=[d]\boldsymbol{N}^{(e)}$. It should be noted that the components of matrix $\boldsymbol{N}^{(e)}$ and $\boldsymbol{B}^{(e)}$ are given in the appendix.

The finite element model of the governing equations can be obtained by using the Rayleigh-Ritz energy formulation. There are different textbooks (Zienkiewicz et al 2005) that explained this method in detail. Then by utilizing this method to the governing equations, the stiffness and mass element matrices can be described as bellow:

$$\boldsymbol{K}^{(e)}=\int_{V^{(e)}}\boldsymbol{B}^T\boldsymbol{\Lambda}\big(\hat{\boldsymbol{N}}\boldsymbol{\Xi}\big)\boldsymbol{B}\,dV \tag{31}$$

$$\boldsymbol{M}^{(e)}=\int_{V^{(e)}}\boldsymbol{N}^T\big(\hat{\boldsymbol{N}}\Re\big)\boldsymbol{N}\,dV \tag{32}$$

where $V_{(e)}$ is the volume of the element.

Now by assembling the element matrices, the global equations of motion for FG porous of joined truncated conical–cylindrical shell reinforced by graphene platelet cone can be written as:

$$[M]\left\{\ddot{\delta}\right\}+[K]\{\delta\}=0 \tag{33}$$

Solving the system of eigenvalue in Eq. (33), the natural frequencies and mode shapes are obtained.

$$([K]-[M]\omega^2)\{\delta\}=0 \tag{34}$$

Table 1 Convergence study of fundamental natural frequency for joined conical-cylindrical shell; Distribution1 – B.C 1 - $\gamma_{GPL} = 0 \cdot 01$, ($\omega \times 10^3$), $\varphi = 15°$, L1 = L2 = 0.5 m, GPLX, $e_0 = 0.1$

Number of elements for joined conical-cylindrical shell $(n_r^{(e)}, n_z^{(e)})$	15*25	20*30	30*40	35*45
Ω (Hz)	1.7828	1.6873	1.6196	1.6143

Table 2 Comparison of first four natural frequencies of isotropic homogeneous joined shell between the present study and ANSYS Workbench

ω_4	ω_3	ω_2	ω_1	Natural frequency (Hz)
4142	2680	2568	1454	Present
4069	2667	2543	1444	ANSYS Workbench

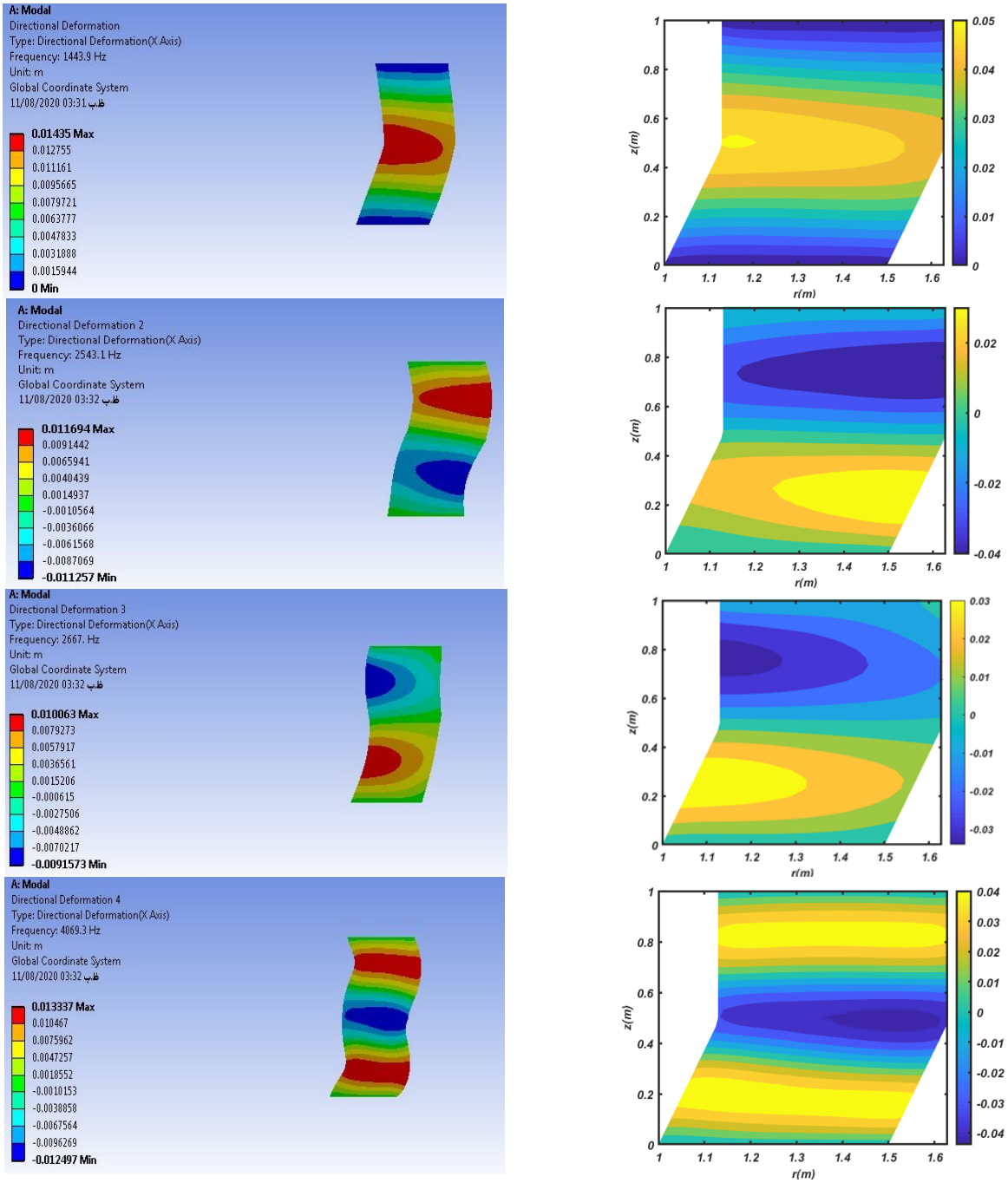

Fig. 2 Comparison of first four mode shapes (u) between present study and ANSYS Workbench

5. Numerical result and discussion

5.1 Convergence study

Convergence of the present research is investigated by comparing results of successive refinement of the element size. In this target, results are compared and reported in Table 1 for different meshes. As can be seen from Table 1, the difference between mesh (30*40) and (35*45) is lower than 1%. Therefore, the 30*40 mesh is chosen for numerical analysis.

5.2 Verification

Example1: Natural frequency analysis of FG porous joined truncated conical–cylindrical shell reinforced by GPLs has not been studied yet. Hence, for confirming the numerical results of the present study, we compared the present numerical results for truncated conical–cylindrical shell made of isotropic homogenous material extracted from ANSYS Workbench commercial FEM software. For this target, it is sufficient to consider $\gamma_{GPL} = 0$ % and $e_0 = 0$, $e_m = 0$ in the present study. Besides, the following material property and geometry are considered:

Geometry:

a = 1 (m), b = 1.5 (m), L1 = 0.5 *(m)*, L2 = 0.5 *(m)*, $\varphi = 15°$.

Material property:

$$\text{E} = 70 \text{ GPa}, \ \rho = 2702(\frac{kg}{m^3}), \upsilon = 0.$$

A compression among the results of the present study and ANSYS Workbench is shown in Fig. 2 and Table 2, and it shows excellent agreement.

Furthermore, two examples are considered to validate the present study with previous-published papers.

Example 2: The present work can be validated using the data of the axisymmetric free vibration of homogeneous isotropic truncated cone based on a 2D axisymmetric finite element model, which was previously published (Thambirantnam and Thevendran 1998). The shell (Conical segment) is clamped on its lower base and the top base is free. For this target, the geometry and material property of the present study should be considered as the following:

Geometry:

a = 1.25 m, b = 1.3125 m, L2 = 0, L1 = 4.17 m, $\varphi = 40°$

These dimensions lead to a truncated cone that has the same geometry as Thambirantnam and Thevendran (1998).

Material property:

$$\text{E} = 30 \text{ GPa}, \ \nu = 0.15, \rho = 2410 \frac{Kg}{m^3}$$

Fundamental natural frequency of truncated cone for various R/L is obtained and compared with the results of Thambirantnam and Thevendran (1998) in Fig 3. The comparison between the results shows an excellent agreement.

Example 3: Besides, the present study may be validated by natural frequencies of an isotopic homogeneous joined cylindrical– conical shell. For this goal, it is sufficient to consider the following non-dimensional geometric and material property parameters:

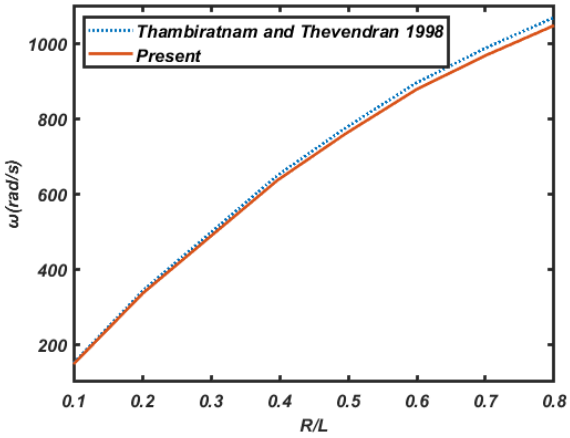

Fig. 3 Comparsion of fundamental natrual frequency for various R/L between present work and Thambirantnam and Thevendran (1998)

Table 3 The comparison of first four natural frequencies of joined shell between present work and Xiang and Matsumoto (2011)

Natural frequency (Hz)	ω_1	ω_2	ω_3	ω_4
Present	0.8701	0.9236	0.9903	1.0328
Xiang and Matsumoto (2011)	0.8705	0.9242	0.9915	1.0346

L1 = L2 = 50, b-a = 1, $\varphi = -15°(\alpha = 15^0)$

$$\text{E} = 10^5, \ \rho = 1$$

The numerical results for the first four natural frequencies of joined shell are obtained and compared with the results of Xiang and Matsumoto (2011) which in Table 3. The shell is clamped on its two end bases. The comparison between results of present study and Xiang and Matsumoto (2011) shows a good agreement.

5.3 Numerical results and discussions

In this section, the results of natural frequency of FG porous joined truncated conical–cylindrical shell reinforced by GPLs have been obtained numerically. The influences of different parameters including porosity coefficient, porosity distributions, GPLs patterns, the weight fraction of nano-fillers, various semi vertex angles, boundary conditions and various length ratios, have been studied. Here the material and geometrical properties of the porous nanocomposite joined truncated conical–cylindrical shell are presented:

Material property:

E_m= 198.8 GPa, ρ_m = 8340 Kg/m3, υ_m = 0.3279 for steel (Smith *et al*. 2012), E_{GPL} = 1.01 TPa, ρ_{GPL} = 1062.5 Kg/m3, υ_{GPL} = 0.186 , w_{GPL} = 1.5 μm, l_{GPL} = 2.5 μm, t_{GPL}= 1.5 nm for GPLs.

Geometrical properties:

a = 1 (m), b = 1.5 (m), L1=0.5 *(m)*, L2=0.5 *(m)*, $\varphi = 15°$

Table 4 Natural frequencies (Hz) of FG porous joined shell reinforced by GPLs for porosity distribution 1 – B.C 1 - $\gamma_{GPL} = 0 \cdot 01$, ($\omega \times 10^3$), $\varphi = 15°$, L1 = L2 = 0.5 m

GPL pattern	Porosity distribution 1						
	e_0	ω_1	ω_2	ω_3	ω_4	ω_5	ω_6
GPLX	0.1	1.6143	2.8298	3.0099	4.5827	4.6575	5.1199
	0.3	1.5523	2.7215	2.8903	4.3792	4.3958	4.8306
	0.5	1.4782	2.5941	2.7513	4.0532	4.1564	4.4801
GPLA	0.1	1.6067	2.802	3.0893	4.5436	4.6047	5.2958
	0.3	1.5445	2.6929	2.9633	4.3408	4.3631	5.0014
	0.5	1.4702	2.5659	2.8166	4.0274	4.1427	4.6311
GPLV	0.1	1.6171	2.8552	2.9714	4.6008	4.7115	5.3843
	0.3	1.5573	2.7493	2.8531	4.42	4.4466	5.0888
	0.5	1.4859	2.6252	2.7156	4.1227	4.2081	4.7232
GPLO	0.1	1.5317	2.7124	2.8034	4.3574	4.4738	5.1775
	0.3	1.4732	2.6087	2.6861	4.1819	4.2212	4.8928
	0.5	1.4033	2.4869	2.5491	3.9079	3.9815	4.5392
GPLUD	0.1	1.6170	2.8546	2.9754	4.6016	4.7095	5.3861
	0.3	1.5572	2.7487	2.8569	4.4205	4.4447	5.09
	0.5	1.4858	2.6246	2.7193	4.1203	4.209	4.7232

Table 5 Natural frequencies (Hz) of FG porous joined shell reinforced by GPLs for porosity distribution 2 – B.C 1 - $\gamma_{GPL} = 0 \cdot 01$, ($\omega \times 10^3$), $\varphi = 15°$, L1 = L2 = 0.5 m

GPL pattern	Porosity distribution 2						
	e_0	ω_1	ω_2	ω_3	ω_4	ω_5	ω_6
GPLX	0.1	1.6143	2.8298	3.0099	4.5827	4.6575	5.1199
	0.3	1.5523	2.7215	2.8903	4.3792	4.3958	4.8306
	0.5	1.4782	2.5941	2.7513	4.0532	4.1564	4.4801
GPLA	0.1	1.6067	2.802	3.0893	4.5436	4.6047	5.2958
	0.3	1.5445	2.6929	2.9633	4.3408	4.3631	5.0014
	0.5	1.4702	2.5659	2.8166	4.0274	4.1427	4.6311
GPLV	0.1	1.6171	2.8552	2.9714	4.6008	4.7115	5.3843
	0.3	1.5573	2.7493	2.8531	4.42	4.4466	5.0888
	0.5	1.4859	2.6252	2.7156	4.1227	4.2081	4.7232
GPLO	0.1	1.5317	2.7124	2.8034	4.3574	4.4738	5.1775
	0.3	1.4732	2.6087	2.6861	4.1819	4.2212	4.8928
	0.5	1.4033	2.4869	2.5491	3.9079	3.9815	4.5392
GPLUD	0.1	1.6170	2.8546	2.9754	4.6016	4.7095	5.3861
	0.3	1.5572	2.7487	2.8569	4.4205	4.4447	5.09
	0.5	1.4858	2.6246	2.7193	4.1203	4.209	4.7232

Tables 4 and 5 show the impact of porosity coefficient and various GPL patterns on the natural frequencies of FG porous joined truncated conical–cylindrical shell reinforced by GPLs for porosity distribution 1 and 2, respectively (B.C 1 - $\gamma_{GPL} = 0 \cdot 01$, $\varphi = 15°$). It is found that by raising the porosity coefficient in all GPL patterns, natural frequencies of both porosity distributions decrease. This is due to the fact that by increasing the pores density, the stiffness and mass matrices of joined shell decrease, but the reduction of stiffness matrix of structure is higher than mass matrix of joined shell. Natural frequencies of all GPL patterns except GPLO are almost identical, and the minimum values of natural frequencies belong to GPLO. In other words, for porosity distribution 1 and 2, when the volume content of GPLs around the mid-thickness of the structure is high, the stiffness of plate reaches its minimum level. Also, results of these two tables denote that natural frequencies of distribution 1 and 2 are almost identical for all GPL patterns.

Table 6 Natural frequencies (Hz) of FG porous joined shell reinforced by GPLs for porosity distribution 3 – B.C 1 - $\gamma_{GPL} = 0 \cdot 01$, ($\omega \times 10^3$), $\varphi = 15°$, L1 = L2 = 0.5 m

GPL pattern	Porosity distribution 1						
	e_0	ω_1	ω_2	ω_3	ω_4	ω_5	ω_6
GPLX	0.1	1.6233	2.8453	3.03	4.6124	4.7254	5.1795
	0.3	1.5638	2.7411	2.9191	4.4436	4.5524	4.99
	0.5	1.4949	2.6203	2.7904	4.2477	4.3517	4.7699
GPLA	0.1	1.6156	2.8173	3.1126	4.5691	4.6649	5.3558
	0.3	1.5565	2.7142	2.9987	4.4019	4.4942	5.1598
	0.5	1.4879	2.5945	2.8665	4.2078	4.296	4.9322
GPLV	0.1	1.6254	2.8704	2.9910	4.6275	4.7768	5.4516
	0.3	1.5659	2.7654	2.8815	4.4582	4.602	5.252
	0.5	1.4968	2.6434	2.7544	4.2616	4.399	5.0205
GPLO	0.1	2.2347	3.9719	4.0332	6.2921	6.451	7.642
	0.3	2.1529	3.8265	3.8856	6.0618	6.2149	7.3623
	0.5	2.058	3.6578	3.7142	5.7945	5.9408	7.0377
GPLUD	0.1	1.617	2.8552	2.9797	4.6046	4.7504	5.4257
	0.3	1.5578	2.7507	2.8706	4.4361	4.5765	5.2271
	0.5	1.4891	2.6294	2.7441	4.2405	4.3747	4.9966

Table 7 Natural frequencies (Hz) of FG porous joined shell reinforced by GPLs for porosity distribution 4 – B.C 1 - $\gamma_{GPL} = 0 \cdot 01$, ($\omega \times 10^3$), $\varphi = 15°$, L1 = L2 = 0.5 m

GPL pattern	Porosity distribution 4						
	e_0	ω_1	ω_2	ω_3	ω_4	ω_5	ω_6
GPLX	0.1	1.5105	2.6548	2.8048	4.2976	4.4102	4.903
	0.3	1.3892	2.4446	2.5692	3.952	4.0681	4.517
	0.5	1.2372	2.1793	2.2762	3.5154	3.6485	4.0354
GPLA	0.1	1.389	2.4508	2.583	3.9623	4.0698	4.6705
	0.3	1.2776	2.2589	2.3633	3.6485	3.7562	4.4566
	0.5	1.2988	2.291	2.407	3.5887	3.6863	4.1301
GPLV	0.1	1.5856	2.8023	2.9107	4.5154	4.6652	5.3149
	0.3	1.4579	2.5807	2.6603	4.1523	4.3072	4.8789
	0.5	1.2982	2.3001	2.3511	3.6942	3.8685	4.334
GPLO	0.1	1.5434	2.7381	2.8187	4.3937	4.5521	5.2576
	0.3	1.4191	2.5225	2.5726	4.0407	4.2053	4.8136
	0.5	1.2635	2.2483	2.2704	3.5956	3.7804	4.2587
GPLUD	0.1	1.5882	2.8066	2.9196	4.5239	4.671	5.3262
	0.3	1.4604	2.5849	2.6687	4.1607	4.3125	4.8903
	0.5	1.3005	2.3043	2.3586	3.7025	3.8731	4.3453

That is because the distribution of pores in the thickness of structure is symmetric, and the ratio of stiffness to mass of structure is almost the same regardless the concentration of pores, which are located near the mild thickness or near the inner and outer of surface.

Table 6 indicates the influence of porosity coefficient and various GPL patterns on natural frequencies for porosity distribution 3 (B.C 1 - $\gamma_{GPL} = 0 \cdot 01$, $\varphi = 15°$). By raising the porosity coefficient of all the GPL patterns, natural frequencies reduce since both stiffness and mass matrices of structure decrease. But, the reduction ratio of stiffness matrix is more than mass matrix. The maximum value of natural frequencies belongs to GPLO. In distribution 3, GPLO has a more significant impact on natural frequencies than other GPL patterns. For GPLO, the values of natural frequencies are approximately 40% greater than those of other GPL patterns. Besides, the value of natural frequencies of GPL-X, V, A and UD are almost

Table 8 Natural frequencies (Hz) of FG porous joined shell reinforced by GPLs for GPLA – B.C 1 - $e_0 = 0 \cdot 4$ - $\gamma_{GPL} = 0 \cdot 01$, (ω×$10^3$), $\varphi = 15°$,L1 = L2 = 0.5

	ω_1	ω_2	ω_3	ω_4	ω_5	ω_6
D1	1.5093	2.6321	2.8931	4.1926	4.2583	4.8286
D2	1.5186	2.6786	2.9756	4.3282	4.7207	5.3124
D3	1.5236	2.6568	2.9353	4.3089	4.3993	5.0508
D4	1.2123	2.1458	2.2351	3.4633	3.5754	4.076

Table 9 Natural frequencies (Hz) of FG porous joined shell reinforced by GPLs for distribution 2- $e_0 = 0 \cdot 4$ – B.C 1 - $\gamma_{GPL} = 0 \cdot 01$, (ω×$10^3$), $\varphi = 15°$, L1 = L2 = 0.5 m

	ω_1	ω_2	ω_3	ω_4	ω_5	ω_6
GPLX	1.5232	2.6887	2.8851	4.3671	4.8441	5.1832
GPLA	1.5186	2.6786	2.9756	4.3282	4.7207	5.3124
GPLV	1.517	2.7	2.8512	4.3498	4.8449	5.3953
GPLO	1.4447	2.5781	2.7133	4.1392	4.6055	5.1886
GPLUD	1.5172	2.7	2.8548	4.3509	4.8437	5.3984

Table 10 Natural frequencies (Hz) of FG porous joined shell reinforced by GPLs for distribution 1 – GPLX - $e_0 = 0 \cdot 4$ – B.C1 , (ω×10^4), $\varphi = 15°$, L1 = L2 = 0.5 m

	ω_1	ω_2	ω_3	ω_4	ω_5	ω_6
$\gamma_{GPL} = 0$	1.2928	2.2826	2.3688	3.6381	3.6707	4.1738
$\gamma_{GPL} = 0 \cdot 005$	1.4115	2.4823	2.6104	3.9473	3.9964	4.4346
$\gamma_{GPL} = 0 \cdot 01$	1.5171	2.6608	2.8237	4.2249	4.2838	4.6644

Table 11 Natural frequencies of FG porous joined shell reinforced by GPLs for distribution 1 – GPLX – B.C1 - $\gamma_{GPL} = 0 \cdot 01$, (ω×$10^3$) - $e_0 = 0 \cdot 4$, L1 = L2 = 0.5 m

	ω_1	ω_2	ω_3	ω_4	ω_5	ω_6
$\varphi = 0°$	1.6101	2.8192	3.0404	4.5919	4.8477	5.2098
$\varphi = 15°$	1.5523	2.7215	2.8903	4.3792	4.3958	4.8306
$\varphi = 30°$	1.528	2.6217	2.7691	4.2777	4.3538	4.8606
$\varphi = 60°$	1.3418	2.1192	2.5794	3.77	3.9191	5.0581

identical. It means if nano filler dispersion concentrates around the inner or outer radius of the shell or disperses uniformly, the structures will have the same ratio of stiffness to mass.

Table 7 indicates the influence of porosity coefficient and various GPL patterns on the natural frequencies for porosity distribution 4 (B.C 1 - $\gamma_{GPL} = 0 \cdot 01$, $\varphi = 15°$). It can be seen that by increasing the porosity coefficient in all GPL patterns except GPLA, natural frequencies decrease. For GPL-A, natural frequencies show a nonlinear behavior. It is observed that by increasing the porosity coefficient from $e_{0=}$ 0.3 to $e_{0=}$ 0.5, natural frequencies increase, because in this case, both stiffness and mass matrices decrease, but the rate of reduction of stiffness matrix is less than mass matrix. The maximum value of natural frequency belongs to GPL UD, GPLV, GPLO, GPLX and GPLA, respectively. In GPL UD nano-fillers are distributed uniformly, and in GPLA the concentration of nano-filler dispersion are mostly in the outer surface of joined shell. These two types of distributions in conjunction with porosity distribution 4 lead to the maximum and minimum value of natural frequencies.

Table 8 shows the effect of porosity distribution on natural frequencies for shell with GPLA, B.C. 1, $e_0 = 0 \cdot 4$, $\gamma_{GPL} = 0 \cdot 01$, $\varphi = 15°$. As can be seen, the minimum value of natural frequency belongs to porosity distribution 4. In this case, the minimum ratio of stiffness to mass is obtained. The maximum difference between natural frequencies of various porosity distributions is 25%.

Table 9 presents the effect of GPL patterns on natural frequencies of porosity distribution 2. It is observed that GPLO has the most effect on the value of natural frequencies, while other GPL patterns have approximately the same value. Also, natural frequency of GPLO is 6% lower than other GPL patterns. Consequently, the GPL-UD can be used in practical application because of the easier fabrication of this pattern rather than other distributions, and also there is not significant difference between the amount of natural frequencies of this GPL pattern and other ones.

Table 12 Natural frequencies of FG porous joined shell reinforced by GPLs for distribution 1 – GPLX – $\varphi = 15°$ - $\gamma_{GPL} = 0 \cdot 01$, (ω×$10^3$), $e_0 = 0 \cdot 4$, L1 = L2 = 0.5 m

	ω_1	ω_2	ω_3	ω_4	ω_5	ω_6
(BC1)	1.5523	2.7215	2.8903	4.3792	4.3958	4.8306
(BC2)	1.5548	2.7936	3.0329	3.1418	3.5393	4.0884
(BC3)	3.3962	3.5292	3.9665	5.0392	5.903	6.0531

Table 13 Natural frequencies (Hz) of FG porous joined shell reinforced by GPLs for distribution 1 – GPLX – B.C1 - $\gamma_{GPL} = 0 \cdot 01$, (ω×$10^3$), $e_0 = 0 \cdot 3, \varphi = 15°$

	ω_1	ω_2	ω_3	ω_4	ω_5	ω_6
$\frac{l2}{l1} = 1$	1.5523	2.7215	2.8903	4.3792	4.3958	4.8306
$\frac{l2}{l1} = 2$	1.5565	2.7114	2.9306	4.3848	4.4301	4.8166
$\frac{l2}{l1} = 5$	1.5556	2.719	2.9576	4.4044	4.4667	4.8457

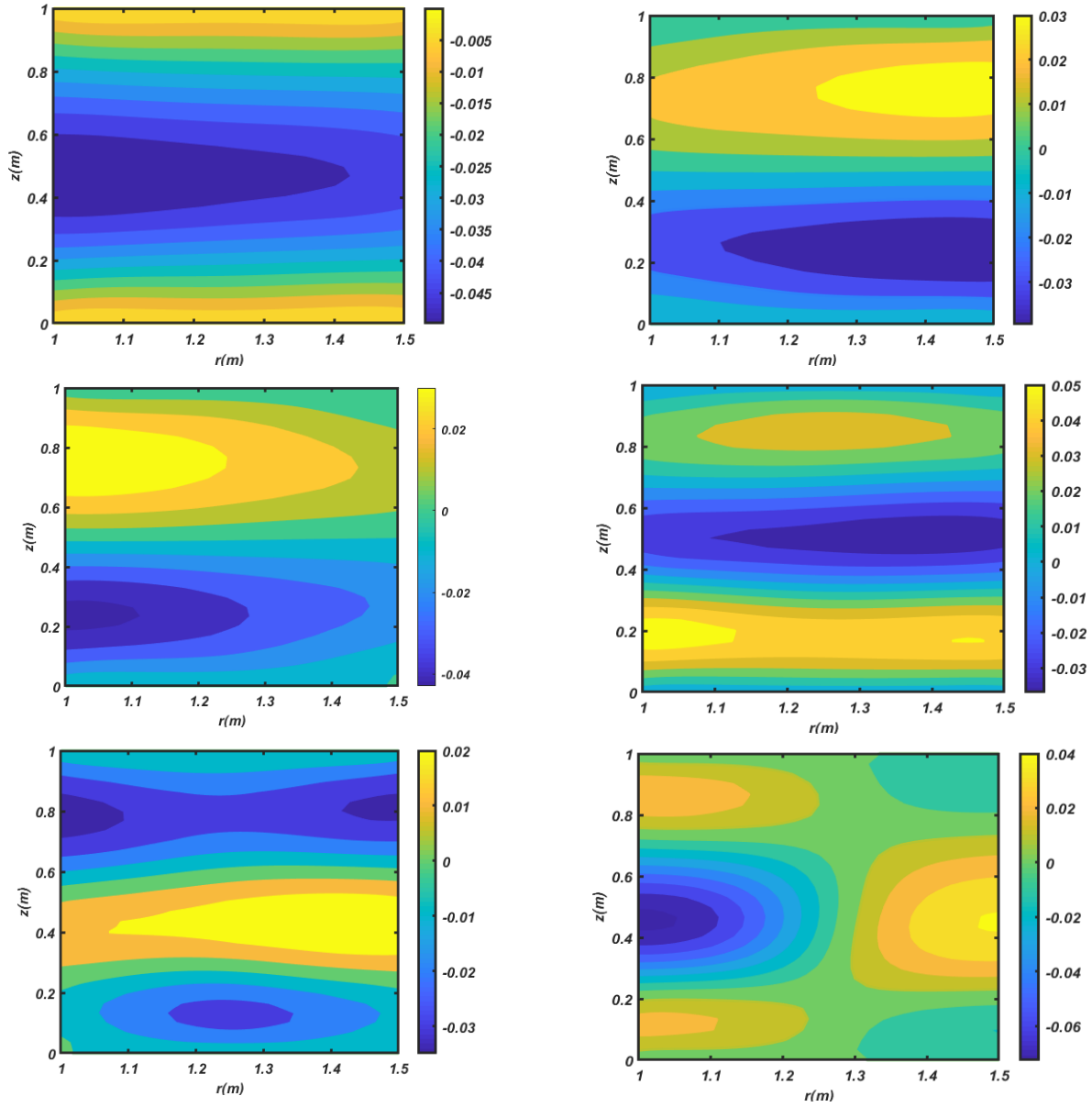

Fig. 4 The first six mode shapes of shell (Distribution 1, GPLX, B.C 1, $\gamma_{GPL} = 0 \cdot 01$, (ω×$10^3$), $\varphi = 0°$)

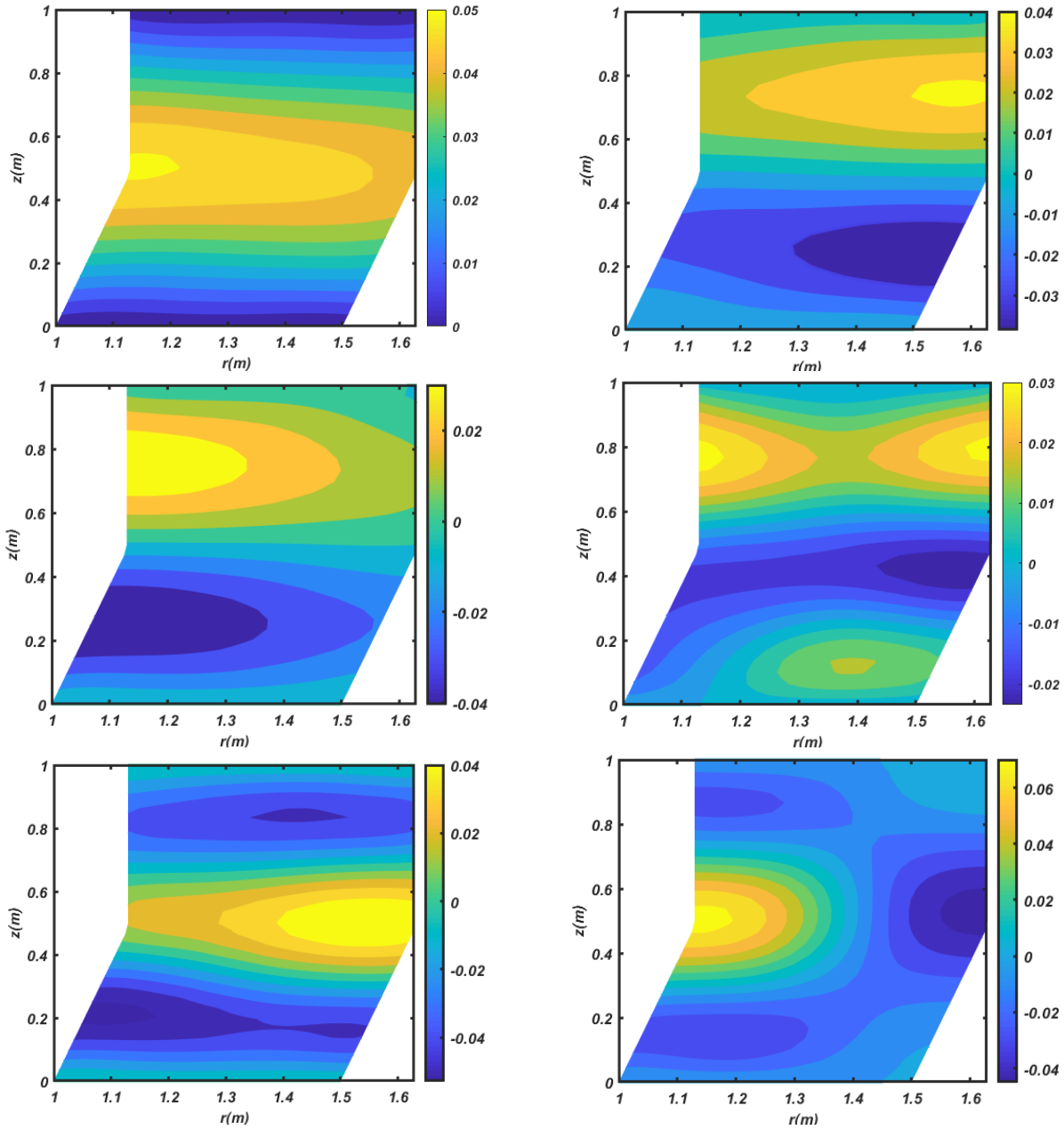

Fig. 5 The first six mode shapes of shell (Distribution 1, GPLX, B.C 1, $\gamma_{GPL} = 0 \cdot 01$, ($\omega \times 10^3$), $\varphi = 15°$)

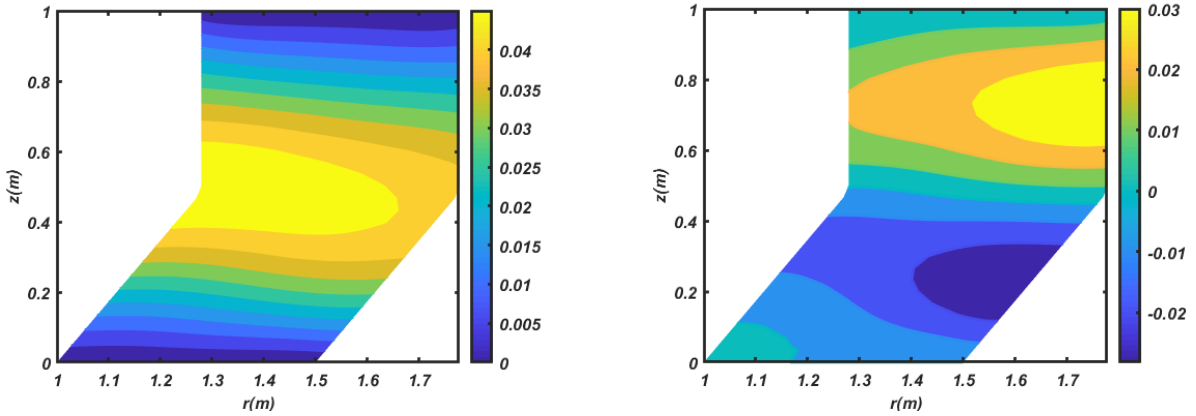

Fig. 6 The first six mode shapes of shell (Distribution 1, GPLX, B.C 1, $\gamma_{GPL} = 0 \cdot 01$, ($\omega \times 10^3$), $\varphi = 30°$)

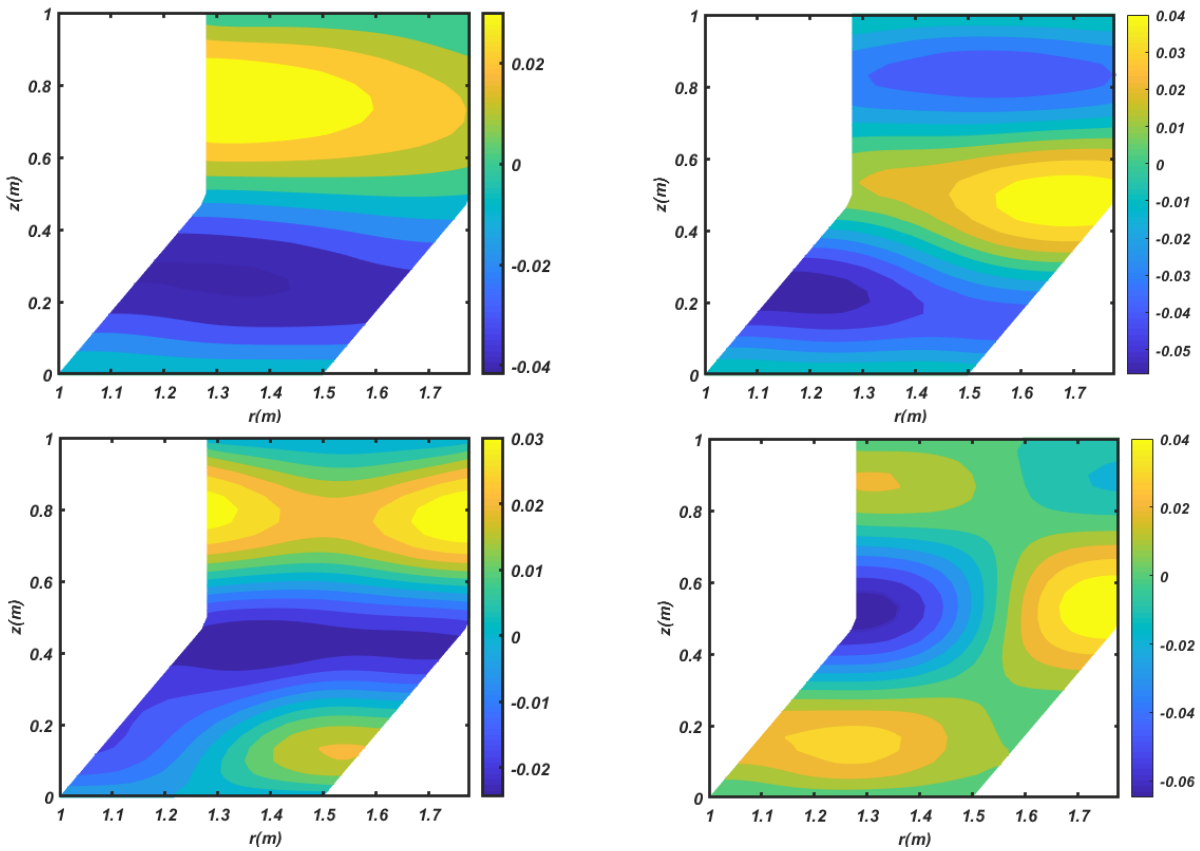

Fig. 6 Continued

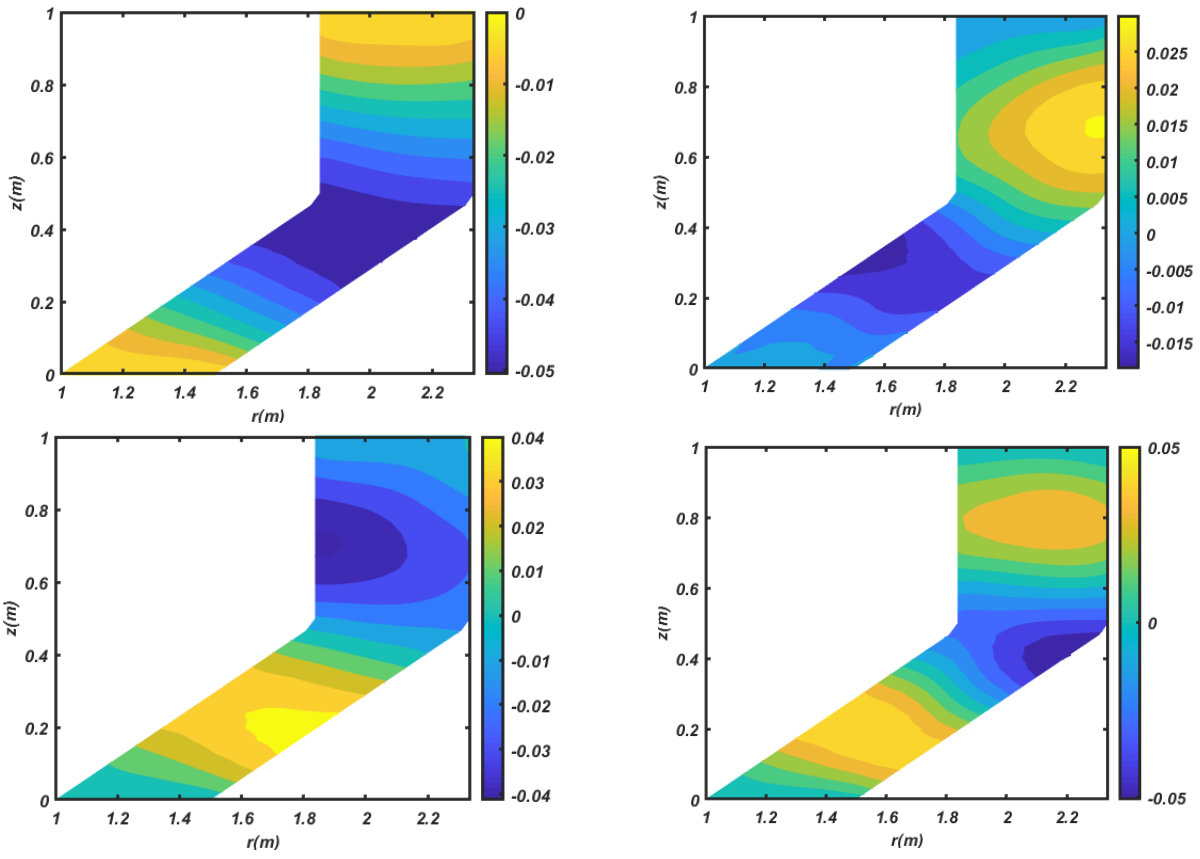

Fig. 7 The first six mode shapes of shell (Distribution 1, GPLX, B.C 1, $\gamma_{GPL} = 0 \cdot 01$, ($\omega \times 10^3$), $\varphi = 60°$)

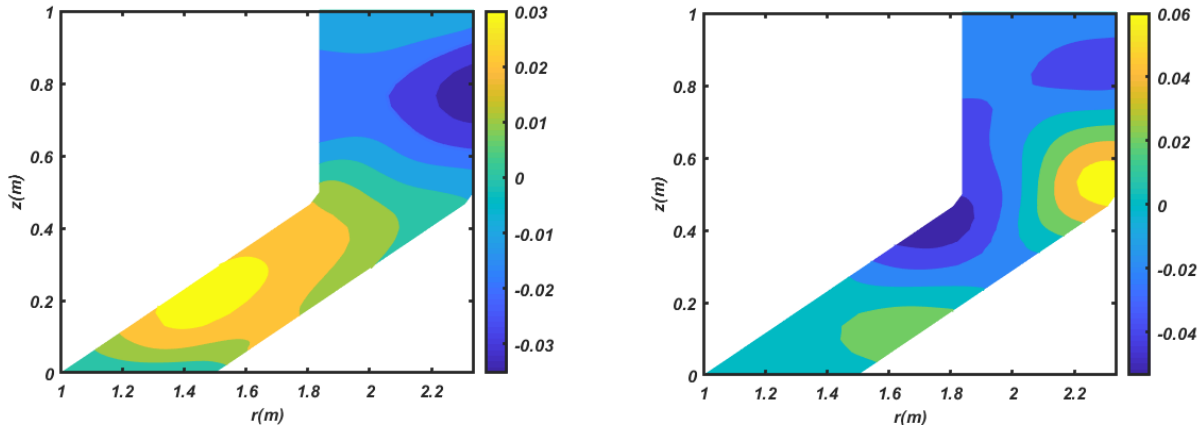

Fig. 7 Continued

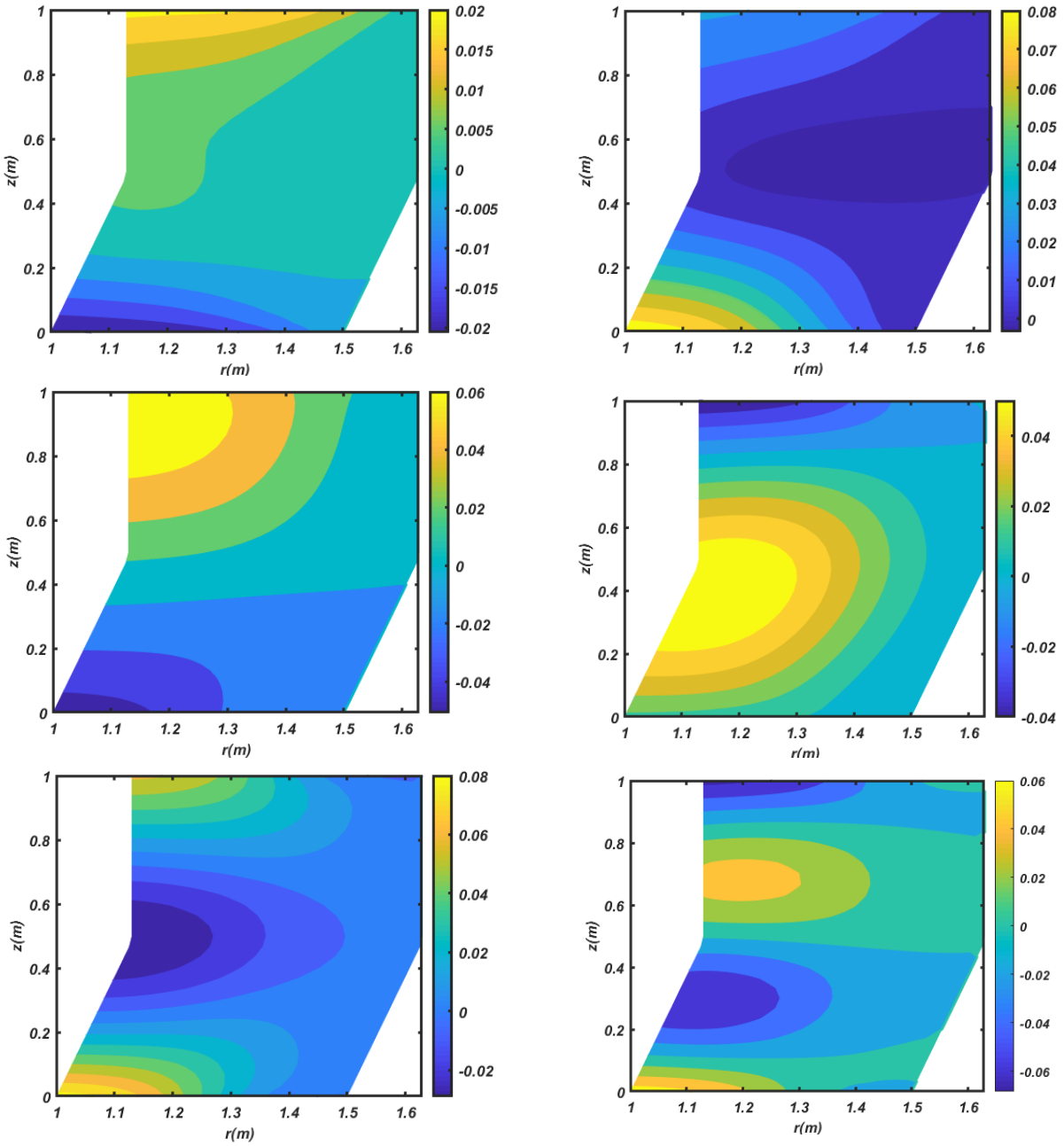

Fig. 8 The first six mode shapes of shell (Distribution 1, GPLX, B.C 2, $\gamma_{GPL} = 0 \cdot 01$, ($\omega \times 10^3$), $\varphi = 15°$)

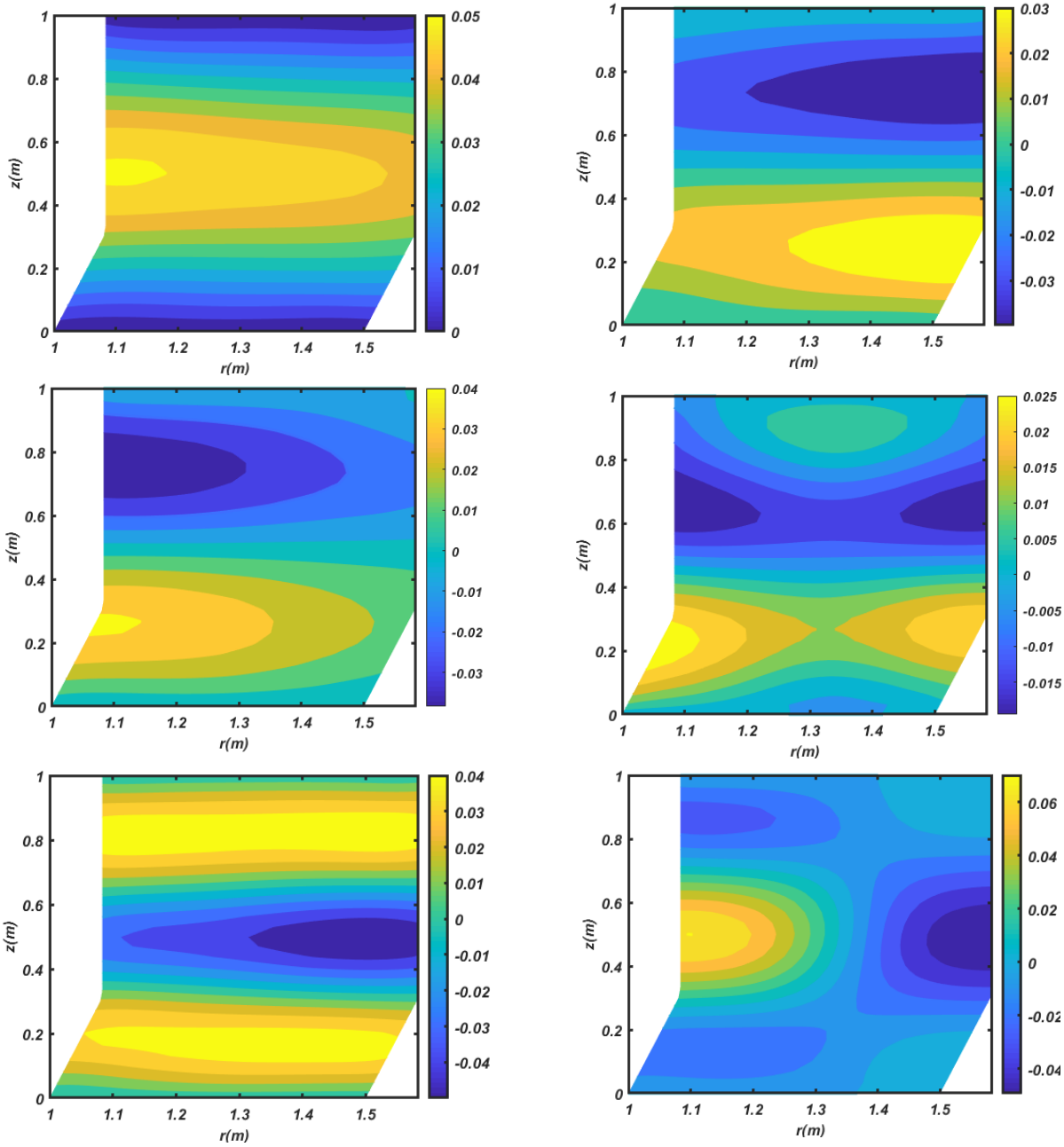

Fig. 9 The first six mode shapes of shell (Distribution 1, GPLX, B.C 1, $\gamma_{GPL} = 0 \cdot 01$, ($\omega \times 10^3$), $\varphi = 15°$, L2 = 2 L1)

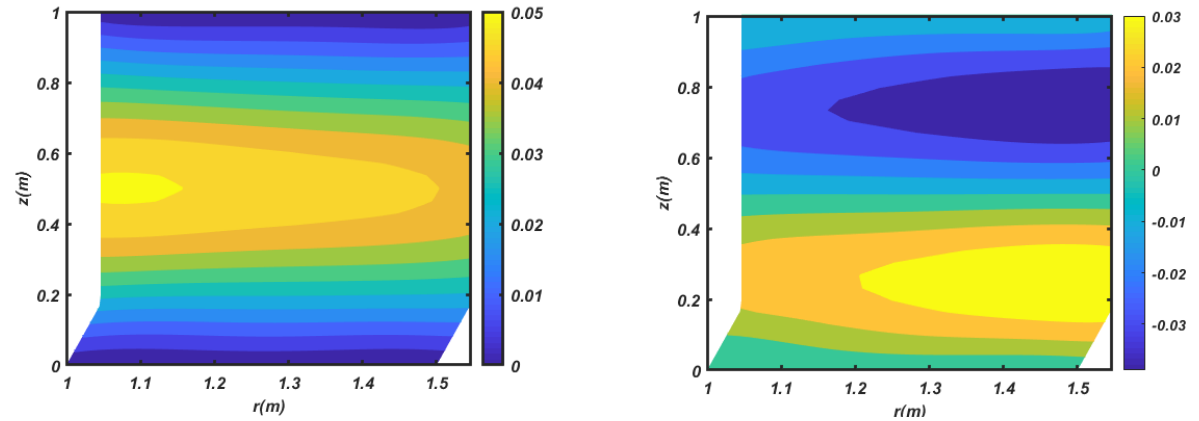

Fig. 10 The first six mode shapes of shell (Distribution 1, GPLX, B.C 1, $\gamma_{GPL} = 0 \cdot 01$, ($\omega \times 10^3$), $\varphi = 15°$, L2 = 5 L1)

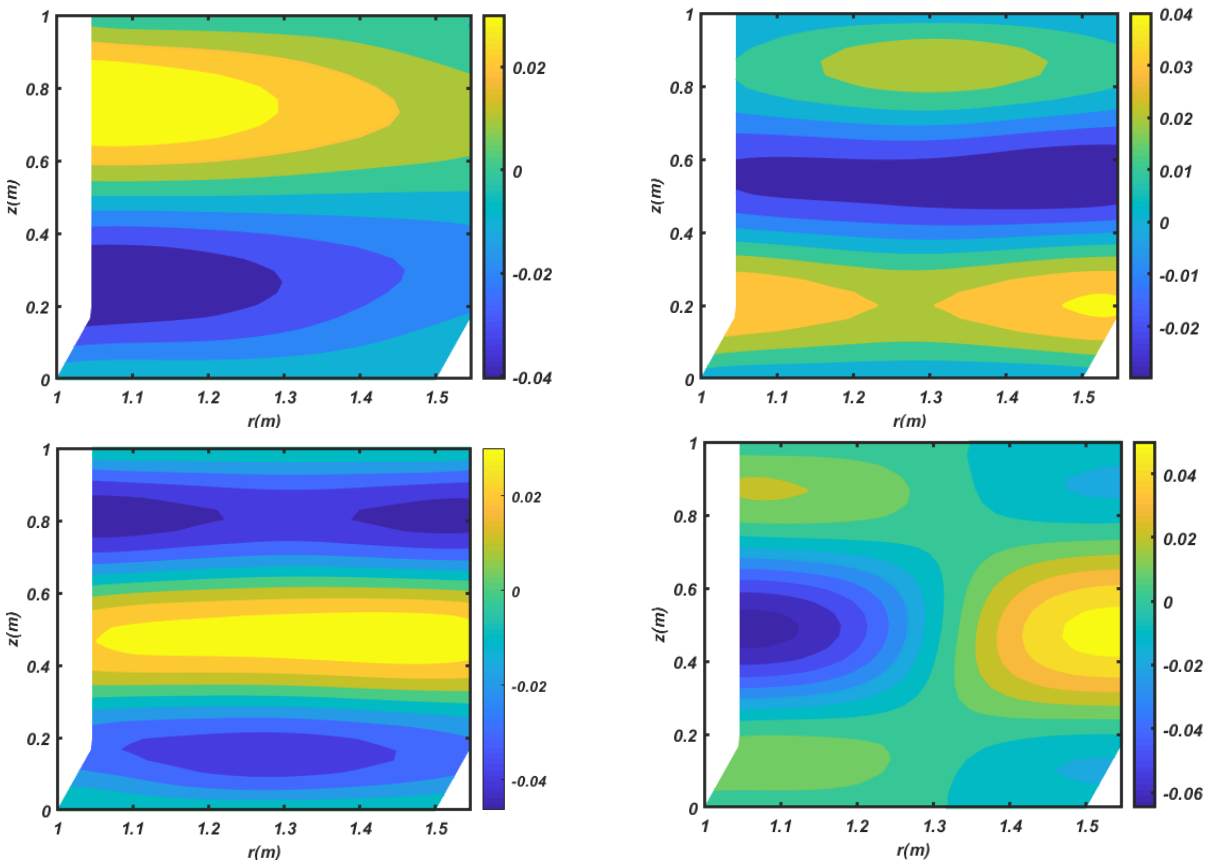

Fig. 10 Continued

The influence of weight fraction of nano-filler is given in Table 10. When weight fraction of nano filler increases from 0 to $0 \cdot 01$, the natural frequencies rise about 17%, since by dispersing the nano fillers into metal matrix, the stiffness of structure significantly increases while the density of nanocomposite doesn't change considerably.

The effect of semi vertex angle of conical shell segment is shown in Table 11. By increasing the semi vertex angle of conical shell from $\varphi = 0°$ to $60°$, natural frequencies decrease 27% approximately due to decreasing the overall stiffness of joined shells.

The influence of boundary condition of shell is given in Table 12. It is obvious that the maximum natural frequency belongs to B.C 3 due to more rigidity of B.C. 3 than other boundary conditions. Also, B.C 1 and B.C 2 have approximately the same value of fundamental frequency.

Table 13 shows the effect of length ratio of structure (length of conical shell per cylindrical shell). It is clear that the length ratio of structure has not considerable effect on natural frequency of structure. The six first mode shapes of shell with B.C 1 for different semi vertex angle $\varphi = 0°, 15°, 30°, 60°$ are shown in Figs. 4-7, respectively. Fig 8 shows the first six mode shapes of shell for B.C 2. Also the first six mode shapes of structure for various length ratio are shown in Fig. 9 (L1 = 2 L2) and Fig 10 (L1 = 5 L2).

6. Conclusions

Free vibration based on 2D axisymmetric elasticity theory by employing graded FEM according to Rayleigh-Ritz energy formulation in FG porous joined truncated conical–cylindrical shell reinforced by graphene platelet has been investigated for the first time. The influences of porosity coefficient, various porosity distributions, GPL dispersion pattern, weight fraction of nanofillers, semi vertex angle, boundary condition and length ratio on free vibration of structure have been studied that can be concluded as bellow:

• The B.C 3 has more natural frequencies than other boundary conditions. Also, the value of fundamental natural frequency for B.C 1 and B.C 2 are approximately the same.

• Porosity distribution 3 and GPLO has the highest natural frequency due to provides the best rigidity.

• Natural frequencies are decreased totally while the porosity coefficient increases, except for porosity distribution 4 and GPLA.

• While the weight fraction of nano-fillers is increased from 0 to 0.01, natural frequencies are approximately increased by 25%.

• By raising the semi vertex angle, natural frequencies are generally decreased.

• The length ratio of structure has not considerable effect on natural frequencies.

• Natural frequencies of porosity distribution 1 and 2 and for all GPL patterns except GPLO are almost identical, and the minimum values of natural frequencies belong to GPLO.

• In porosity distribution 3 and for GPLO, the values of

natural frequencies are approximately 40% greater than those of other GPL patterns.

• For porosity distribution 4 and GPLA, natural frequencies show a nonlinear behavior with respect to porosity coefficient.

References

Akbaş, S.D. (2017a), "Stability of a non-homogenous porous plate by using generalized differantial quadrature method", *Int. J. Eng. Appl. Sci.*, **9**(2), 147-155. https://doi.org/10.24107/ijeas.322375.

Akbaş, S.D. (2017b), "Post-buckling responses of functionally graded beams with porosities", *Steel Compos. Struct.*, **24**(5), 579-589. https://doi.org/10.12989/scs.2017.24.5.579.

Akbaş, S.D. (2017c), "Thermal effects on the vibration of functionally graded deep beams with porosity", *Int. J. Appl. Mech.*, **9**(5), 1750076. https://doi.org/10.1142/S1758825117500764.

Akbaş, S.D. (2017d), "Vibration and static analysis of functionally graded porous plates", *J. Appl. Comput. Mech.*, **3**(3), 199-207. https://doi.org/10.22055/jacm.2017.21540.1107

Akbaş, S.D. (2018a), "Geometrically nonlinear analysis of functionally graded porous beams", *Wind Struct.*, **27**(1), 59-70. http://doi.org/10.12989/was.2018.27.1.059.

Akbaş, S.D. (2018b), "Forced vibration analysis of functionally graded porous deep beams", *Compos. Struct.*, **186**, 293-302. https://doi.org/10.1016/j.compstruct.2017.12.013.

Asemi, K., Salehi, M. and Akhlaghi, M. (2014), "Transient thermal stresses in functionally graded thick truncated cones by graded finite element method", *Int. J. Press. Vessel*, **119**, 52-61. https://.doi.org/10.1016/j.ijpvp.2014.03.002.

Asemi, K., Babaei, M. and Kiarasi, F. (2020), "Static, natural frequency and dynamic analyses of functionally graded porous annular sector plates reinforced by graphene platelets", *Mech. Based Des. Struct.*, 1-29. https://doi.org/10.1080/15397734.2020.1822865.

Ashby, M.F., Evans, T., Fleck, N.A., Hutchinson, J., Wadley, H. and Gibson, L. (2000), *Metal foams: A design guide*, Elsevier.

Asgari, M. (2015), "Two dimensional functionally graded material finite thick hollow cylinder axisymmetric vibration mode shapes analysis based on exact elasticity theory", *J. Theor. Appl. Mech.*, **45**(2), https://doi.org/3.10.1515/jtam-2015-0008.

Babaei, M., Asemi, K., Safarpour, P. (2019), "Natural frequency and dynamic analyses of functionally graded saturated porous beam resting on viscoelastic foundation based on higher order beam theory", *J. Solid Mech.*, **11**(3), 615-634. https://doi: 10.22034/jsm.2019.666691.

Babaei, M. and Asemi, K. (2020), "Stress analysis of functionally graded saturated porous rotating thick truncated cone", *Mech. Based Des. Struct.*, 1-28. https://doi.org/10.1080/15397734.2020.1753536.

Babaei, M., Asemi, K. and Kiarasi, F. (2020), "Static response and free-vibration analysis of a functionally graded annular elliptical sector plate made of saturated porous material based on 3D finite element method", *Mech. Based Des. Struct.*, 1-25. https://doi.org/10.1080/15397734.2020.1864401.

Babaei, M., Asemi, K. and Kiarasi, F. (2021) "Dynamic analysis of functionally graded rotating thick truncated cone made of saturated porous materials", *Thin Wall. Struct.*, **164**, 107852. https://doi.org/10.1016/j.tws.2021.107852.

Bagheri, H., Kiani, Y. and Eslami, M.R. (2017), "Free vibration of joined conical-conical shells", *Thin Wall. Struct.*, **120**, 446-457. https://doi.org/10.1016/j.tws.2017.06.032.

Bagheri, H., Kiani, Y. and Eslami, M.R. (2018), "Free vibration of joined conical–cylindrical–conical shells", *Acta Mech*, **229**, 2751-2764. https://doi.org/10.1007/s00707-018-2133-3

Bagheri, H., Kiani, Y., Bagheri, N. and Eslami, M.R. (2020), "Free vibration of joined cylindrical–hemispherical FGM shells", *Arch. Appl. Mech.*, **90**, 2185-2199. https://doi.org/10.1007/s00419-020-01715-1.

Bahaadini, R., Saidi, A.R., Arabjamaloei, Z. and Ghanbari-Nejad-Parizi, A. (2019), "Vibration analysis of functionally graded graphene reinforced porous nanocomposite shells", *Int. J. Appl. Mech.*, **11**(7)- 1580-1588. doi:10.1142/S1758825119500686.

Besseghier, A., Heireche, H., Bousahla, A.A., Tounsi, A. and Benzair, A. (2015), "Nonlinear vibration properties of a zigzag single-walled carbon nanotube embedded in a polymer matrix", *Adv. Nano Res.*, **3**(1), 29-37. http://doi.org/10.12989/anr.2015.3.1.029.

Chen, M., Xie, K., Jia, W. and Xu, K. (2015), "Free and forced vibration of ring-stiffened conical–cylindrical shells with arbitrary boundary conditions", *Ocean Eng.*, **108**(1), 241-256. https://doi.org/10.1016/j.oceaneng.2015.07.065.

Choi, J., Lakes, R. (1995), "Analysis of elastic modulus of conventional foams and of re-entrant foam materials with a negative poisson's ratio", *Int. J. Mech. Sci.*, **37**(1), 51-59. https://doi.org/10.1016/0020-7403(94)00047-N.

Dong, Y.H., Li, Y.H., Chen, D. and Yang, J. (2018), "Vibration characteristics of functionally graded graphene reinforced porous nanocomposite cylindrical shells with spinning motion", *Compos. Part B Eng.*, **145**, 1-13. https://doi.org/10.1016/j.compositesb.2018.03.009.

Duarte, I., Ventura, E., Olhero, S. andFerreira, J. M. (2015), "An effective approach to reinforced closed-cell Al-alloy foams with multiwalled carbon nanotubes", *Carbon*, **95**, 589-600. https://doi.org/10.1016/j.carbon.2015.08.065.

Ebrahimi, F., Seyfi, A., Dabbagh, A. and Tornabene, F. (2019), "Wave dispersion characteristics of porous graphene platelet-reinforced composite shells", *Struct. Eng. Mech.*, **71**(1), 99-107. http://doi.org/10.12989/sem.2019.71.1.099.

Gao, K., Gao, W., Chen, D. and Yang, J. (2018), "Nonlinear free vibration of functionally graded graphene platelets reinforced porous nanocomposite plates resting on elastic foundation", *Compos. Struct.*, **204**, 831-846. https://doi.org/10.1016/j.compstruct.2018.08.013.

Gia Ninh, D., Tri Minh, V., Van Tuan, N., Chi Hung, N. and Van Phong, D. (2020), "Novel numerical approach for free vibration of nanocomposite joined conical–cylindrical–conical shells", *AIAA J.*, **59**(1), 366-378. https://doi.org/10.2514/1.J059518.

Gibson, L.J., Ashby, M. (1982), "The mechanics of three-dimensional cellular materials", *Proc. Math. Phys. Eng. Sci.*, **382**(1782), 43-59. https://doi.org/10.1098/rspa.1982.0088.

Hassani, A., Habibolahzadeh, A. and Bafti, H. (2012), "Production of graded aluminum foams via powder space holder technique", *Mater. Des.*, **40**, 510-515. https://doi.org/10.1016/j.matdes.2012.04.024.

Hussain, M., Naeem, M.N., Taj, M. and Tounsi, A. (2020a), "Simulating vibration of single-walled carbon nanotube using Rayleigh-Ritz's method", *Adv. Nano Res.*, **8**(3), 215-228. http://doi.org/10.12989/anr.2020.8.3.215.

Hussain, M., Naeem, M. N. and Tounsi, A. (2020b), "Response of orthotropic Kelvin modeling for single-walled carbon nanotubes: Frequency analysis", *Adv. Nano Res.*, **8**(3), 229-244. http://doi.org/10.12989/anr.2020.8.3.229.

Iijima, S. (1991), "Helical microtubules of graphitic carbon", *Nature*, **354**(6348), 56-58. https://doi.org/10.1038/354056a0.

Irie T., Yamada G. and Muramoto Y. (1984), "Free vibration of joined conical-cylindrical shells", *J. Sound Vib.*, **95** (1), 31-39. https://doi.org/10.1016/0022-460X(84)90256-6.

Kang, J.H. (2012), "Three-dimensional vibration analysis of joined thick conical–cylindrical shells of revolution with variable thickness", *J. Sound Vib.*, **331**(18), 4187-4198.

https://doi.org/10.1016/j.jsv.2012.04.021.
Khadimallah, M.A., Hussain, M., Khedher, K.M., Bouzgarrou, S.M., Al Naim, A.F., Naeem, M.N. and Tounsi, A. (2020), "Vibration of SWCNTs: Consistency and behavior of polynomial law index with Galerkin's model", *Adv. Nano Res.*, **9**(4), 251-261. http://doi.org/10.12989/anr.2020.9.4.251
Khosravi, F., Simyari, M., Hosseini, S.A. and Tounsi, A. (2020), "Size dependent axial free and forced vibration of carbon nanotube via different rod models", *Adv. Nano Res.*, **9**(3), 157-172. http://doi.org/10.12989/anr.2020.9.3.157.
Lee, J. (2018), "Free vibration analysis of joined conical-cylindrical shells by matched Fourier-Chebyshev collocation method", *J. Mech. Sci. Technol.*, **32**(10), 4601-4612. https://doi.org/10.1007/s12206-018-0907-0.
Lefebvre, L.P., Banhart, J. and Dunand, D.C. (2008), "Porous metals and metallic foams: current status and recent developments", *Adv. Eng. Mater.*, **10**(9), 775-787. https://doi.org/10.1002/adem.200800241.
Leissa, A.W. (1993), *Vibration of Shells*, American Institute of Physics, New York, U.S.A.
Liew, K.M., Lei, Z.X. and Zhang, L.W. (2015), "Mechanical analysis of functionally graded carbon nanotube reinforced composites: a *review*", *Compos. Struct.*, **120**, 90-97. https://doi.org/10.1016/j.compstruct.2014.09.041.
Mittal, G., Dhand, V., Rhee, K.Y., Park, S.J. and Lee, W.R. (2015), "A review on carbon nanotubes and graphene as fillers in reinforced polymer nanocomposites", *J. Ind. Eng. Chem.*, **21**, 11-25. https://doi.org/10.1016/j.jiec.2014.03.022.
Nematollahi, M.S., Mohammadi, H., Dimitri, R. and Tornabene, F. (2020), "Nonlinear vibration of functionally graded graphene nanoplatelets polymer nanocomposite sandwich beams", *Appl. Sci.*, **10**(16), 5669. https://doi.org/10.3390/app10165669.
Nguyen, T.N., Thai, C.H., Luu, A.T., Nguyen-Xuan, H. and Lee, J. (2019), "NURBS-based postbuckling analysis of functionally graded carbon nanotube-reinforced composite shells", *Comput. Method Appl. Mech. Eng.*, **347**, 983-1003. https://doi.org/10.1016/j.cma.2019.01.011.
Qatu, M.S. (2004), *Vibration of Laminated Shells and Plates*, Elsevier, New York, U.S.A.
Qu, Y., Chen, Y., Long, X., Hua, H. and Meng, G. (2013), "A variational method for free vibration analysis of joined cylindrical–conical shells", *J. Vib. Control*, **19**(6), 2319-2334. https://doi.org/10.1177/1077546312456227.
Rafiee, M.A., Rafiee, J., Wang, Z., Song, H., Yu, Z.Z. and Koratkar, N. (2009), "Enhanced mechanical properties of nanocomposites at low graphene content", *ACS Nano*, **3**(12), 3884-3890. https://doi.org/10.1021/nn9010472.
Shakouri, M. and Kochakzadeh, M.A. (2014), "Free vibration analysis of joined conical shells analytical and experimental study", *Thin Wall. Struct.*, **85**(1), 350-358. https://doi.org/10.1016/j.tws.2014.08.022.
Shen, H.S., Lin, F. and Xiang, Y. (2017), "Nonlinear vibration of functionally graded graphene-reinforced composite laminated beams resting on elastic foundations in thermal environments", *Nonlinear Dyn.*, **90**, 899-914. https://doi.org/10.1007/s11071-017-3701-0.
Smith, B.H., Szyniszewski, S., Hajjar, J. F., Schafer, B. W. and Arwade, S. R. (2012), "Steel foam for structures: A review of applications, manufacturing and material properties", *J. Constr. Steel Res*, **71**, 1-10. https://doi.org/10.1016/j.jcsr.2011.10.028.
Soedel, W. (2004), *Vibrations of Shells and Plates*, Marcel Dekker, New York, U.S.A. https://doi.org/10.1121/1.1873932.
Soureshjani, A.H., Talebitooti, R. and Talebitooti, M. (2020a), "A semi-analytical approach on the effect of external lateral pressure on free vibration of joined sandwich aerospace composite conical-conical shells", *Aerosp. Sci. Technol.*, **99**, 105559. https://doi.org/10.1016/j.ast.2019.105559.
Soureshjani, A.H., Talebitooti, R. and Talebitooti M., (2020b), "Thermal effects on the free vibration of joined FG-CNTRC conical-conical shells", *Thin Wall. Struct.*, **156**, 106960. https://doi.org/10.1016/j.tws.2020.106960.
Thambiratnam, D.P. and Thevendran, V. (1988), "Optimum design of conical shells for free vibration", *Comput. Struct.*, **29**(1), 133-140. https://doi.org/10.1016/0045-7949(88)90178-2.
Tjong, S.C. (2013), "Recent progress in the development and properties of novel metal matrix nanocomposites reinforced with carbon nanotubes and graphene nanosheets", *Mater. Sci. Eng. R Rep.*, **74**(10), 281-350. https://doi.org/10.1016/j.mser.2013.08.001.
Wang, Y.Q. and Zu, J.W. (2017), "Vibration behaviors of functionally graded rectangular plates with porosities and moving in thermal environment", *Aerosp. Sci. Technol.*, **69**, 550-562. https://doi.org/10.1016/j.ast.2017.07.023
Wicklein, M. and Thoma, K. (2005), "Numerical investigations of the elastic and plastic behaviour of an open-cell aluminium foam", *Mater. Sci. Eng.*, **397**(1-2), 391-399. https://doi.org/10.4028/www.scientific.net/AMM.226-228.3.
Wu, S.H., Qu, Y.G., Huang, X. C. and Hua, H. X. (2012), "Free vibration analysis on combined cylindrical-spherical shell", *Appl. Mech. Mater.*, **226**, 3-8. https://doi.org/10.4028/www.scientific.net/amm.226-228.3
Xia, X. C., Chen, X. W., Zhang, Z., Chen, X., Zhao, W. M., Liao, B. and Hur, B. (2013), "Effects of porosity and pore size on the compressive properties of closed-cell Mg alloy foam", *J. Magnes. Alloy*, **1**(4), 330-335. https://doi.org/10.1016/j.jma.2013.11.006.
Xiang, J. and Matsumoto, T. (2011), "Vibration analysis of conical shell based on wavelet finite element method", *Trans Jascome*, **11**, 101-106.
Yan, K., Zhang, Y., Cai, H. and Tahouneh, V. (2020), "Vibrational characteristic of FG porous conical shells using Donnell's shell theory", *Steel Compos. Struct.*, **35**(2), 249-260. https://doi.org/10.12989/SCS.2020.35.2.249.
Zhao, S., Yang, Z., Kitipornchai, S. and Yang, J. (2020), "Dynamic instability of functionally graded porous arches reinforced by graphene platelets", *Thin Wall. Struct.*, **147**, 106491. https://doi.org/10.1016/j.tws.2019.1r06491.
Zienkiewicz, O.C., Taylor, R.L. and Zhu, J.Z. (2005), *The Finite Element Method: Its Basis and Fundamentals*, Elsevier.

AT

Appendix

$$\boldsymbol{N} = \begin{bmatrix} N_1 & 0 & N_2 & 0 & N_3 & 0 & N_4 & 0 & N_5 & 0 & N_6 & 0 \\ 0 & N_1 & 0 & N_2 & 0 & N_3 & 0 & N_4 & 0 & N_5 & 0 & N_6 \end{bmatrix}$$

$$N_1 = \frac{(r_{23}(z-z_3)-z_{23}(r-r_3))(r_{46}(z-z_6)-z_{46}(r-r_6))}{(r_{23}z_{13}-z_{23}r_{13})(r_{46}z_{16}-z_{46}r_{16})}$$

$$N_2 = \frac{(r_{31}(z-z_1)-z_{31}(r-r_1))(r_{54}(z-z_4)-z_{54}(r-r_4))}{(r_{31}z_{21}-z_{31}r_{21})(r_{54}z_{24}-z_{54}r_{24})}$$

$$N_3 = \frac{(r_{21}(z-z_1)-z_{21}(r-r_1))(r_{56}(z-z_6)-z_{56}(r-r_6))}{(r_{21}z_{31}-z_{21}r_{31})(r_{56}z_{36}-z_{56}r_{36})}$$

$$N_4 = \frac{(r_{31}(z-z_1)-z_{31}(r-r_1))(r_{23}(z-z_3)-z_{23}(r-r_3))}{(r_{31}z_{41}-z_{31}r_{41})(r_{23}z_{43}-z_{23}r_{43})}$$

$$N_5 = \frac{(r_{31}(z-z_1)-z_{31}(r-r_1))(r_{21}(z-z_1)-z_{21}(r-r_1))}{(r_{31}z_{51}-z_{31}r_{51})(r_{21}z_{51}-z_{21}r_{51})}$$

$$N_6 = \frac{\big(r_{21}(z-z_1)-z_{21}(r-r_1)\big)\big(r_{23}(z-z_3)-z_{23}(r-r_3)\big)}{(r_{21}z_{61}-z_{21}r_{61})(r_{23}z_{63}-z_{23}r_{63})}$$

$$\boldsymbol{B} = \begin{bmatrix} \frac{\partial N_1}{\partial r} & 0 & \frac{\partial N_2}{\partial r} & 0 & \frac{\partial N_3}{\partial r} & 0 & \frac{\partial N_4}{\partial r} & 0 & \frac{\partial N_5}{\partial r} & 0 & \frac{\partial N_6}{\partial r} & 0 \\ \frac{1}{r}N_1 & 0 & \frac{1}{r}N_2 & 0 & \frac{1}{r}N_3 & 0 & \frac{1}{r}N_4 & 0 & \frac{1}{r}N_5 & 0 & \frac{1}{r}N_6 & 0 \\ 0 & \frac{\partial N_1}{\partial z} & 0 & \frac{\partial N_2}{\partial z} & 0 & \frac{\partial N_3}{\partial z} & 0 & \frac{\partial N_4}{\partial z} & 0 & \frac{\partial N_5}{\partial z} & 0 & \frac{\partial N_6}{\partial z} \\ \frac{1}{2}\frac{\partial N_1}{\partial z} & \frac{1}{2}\frac{\partial N_1}{\partial r} & \frac{1}{2}\frac{\partial N_2}{\partial z} & \frac{1}{2}\frac{\partial N_2}{\partial r} & \frac{1}{2}\frac{\partial N_3}{\partial z} & \frac{1}{2}\frac{\partial N_3}{\partial r} & \frac{1}{2}\frac{\partial N_4}{\partial z} & \frac{1}{2}\frac{\partial N_4}{\partial r} & \frac{1}{2}\frac{\partial N_5}{\partial z} & \frac{1}{2}\frac{\partial N_5}{\partial r} & \frac{1}{2}\frac{\partial N_6}{\partial z} & \frac{1}{2}\frac{\partial N_6}{\partial r} \end{bmatrix}$$

$$\frac{\partial N_1}{\partial r} = \frac{-z_{23}[r_{46}[z-z_6]-z_{46}[r-r_6]]-z_{46}[r_{23}[z-z_3]-z_{23}[r-r_3]]}{[r_{23}z_{13}-z_{23}r_{13}][r_{46}z_{16}-z_{46}r_{16}]}$$

$$\frac{\partial N_1}{\partial z} = \frac{-r_{23}[r_{36}[z-z_6]-z_{36}[r-r_6]]-r_{46}[r_{13}[z-z_3]-z_{13}[r-r_3]]}{[r_{23}z_{13}-z_{23}r_{13}][r_{46}z_{16}-z_{46}r_{16}]}$$

$$\frac{\partial N_2}{\partial r} = \frac{-z_{31}[r_{54}[z-z_4]-z_{54}[r-r_4]]-z_{54}[r_{31}[z-z_1]-z_{31}[r-r_1]]}{[r_{21}z_{51}-z_{21}r_{51}][r_{21}z_{51}-z_{21}r_{43}]}$$

$$\frac{\partial N_2}{\partial z} = \frac{-r_{31}[r_{54}[z-z_4]-z_{54}[r-r_4]]+r_{54}[r_{21}[z-z_1]-z_{31}[r-r_1]]}{[r_{21}z_{21}-z_{31}r_{21}][r_{54}z_{24}-z_{54}r_{24}]}$$

$$\frac{\partial N_3}{\partial r} = \frac{-z_{21}[r_{56}[z-z_6]-z_{56}[r-r_6]]-z_{56}[r_{21}[z-z_1]-z_{21}[r-r_1]]}{[r_{21}z_{31}-z_{21}r_{31}][r_{56}z_{36}-z_{56}r_{36}]}$$

$$\frac{\partial N_3}{\partial z} = \frac{-r_{21}[r_{56}[z-z_6]-z_{56}[r-r_6]]-r_{56}[r_{21}[z-z_1]-z_{21}[r-r_1]]}{[r_{21}z_{31}-z_{21}r_{31}][r_{56}z_{36}-z_{56}r_{36}]}$$

$$\frac{\partial N_4}{\partial r} = \frac{-z_{21}[r_{23}[z-z_3]-z_{22}[r-r_2]]-z_{23}[r_{31}[z-z_1]-z_{31}[r-r_4]]}{[r_{31}z_{41}-z_{31}r_{41}][r_{23}z_{43}-z_{23}r_{43}]}$$

$$\frac{\partial N_4}{\partial z} = \frac{-r_{21}[r_{23}[z-z_2]-z_{23}[r-r_2]]+r_{23}[r_{21}[z-z_1]-z_{31}[r-r_1]]}{[r_{21}z_{41}-z_{21}r_{41}][r_{23}z_{43}-z_{23}r_{43}]}$$

$$\frac{\partial N_5}{\partial r} = \frac{-z_{31}[r_{21}[z-z_1]-z_{21}[r-r_1]]-z_{21}[r_{31}[z-z_1]-z_{31}[r-r_1]]}{[r_{21}z_{51}-z_{21}r_{51}][r_{21}z_{51}-z_{21}r_{43}]}$$

$$\frac{\partial N_5}{\partial z} = \frac{-r_{51}[r_{21}[z-z_1]-z_{21}[r-r_1]]+r_{21}[r_{21}[z-z_1]-z_{31}[r-r_1]]}{[r_{31}z_{51}-z_{31}r_{51}][r_{21}z_{51}-z_{21}r_{51}]}$$

$$\frac{\partial N_6}{\partial r} = \frac{-z_{21}[r_{23}[z-z_3]-z_{23}[r-r_3]]-z_{21}[r_{21}[z-z_1]-z_{31}[r-r_1]]}{[r_{21}z_{61}-z_{21}r_{61}][r_{23}z_{63}-z_{23}r_{63}]}$$

$$\frac{\partial N_6}{\partial z} = \frac{-r_{21}[r_{23}[z-z_3]-z_{23}[r-r_3]]-r_{23}[r_{31}[z-z_1]-z_{31}[r-r_1]]}{[r_{21}z_{61}-z_{21}r_{61}][r_{23}z_{63}-z_{23}r_{63}]}$$